Norwegian University of Science and Technology
NTNU

Department of Chemical Engineering

Modelling and Optimization of Compact Sub-sea Separators

Master's Thesis

by

Fahad Matovu

Supervisor: Associate Prof. Johannes Jäschke

Co-supervisor: Prof.Sigurd Skogestad

Trondheim, June 9, 2015

Abstract

This Master thesis focuses on Modelling and Optimization of Compact sub-sea separators using a given separation system. The separation system consists of three separation units: a gravity separator, a deliquidizer and a degasser.

The steady state models developed have been aimed at predicting phase separation in the separator units. The models in addition predict stream outlet phase fractions and flow rates based on known inlet conditions and separator geometry.

Model simulations have been performed in Matlab and results have shown trends that are consistent with theoretical expectations. They have in some cases for the deliquidizer been compared to experimental data and close agreement has been observed. However, in other cases, validation of simulation results has not been possible due to lack of experimental data but the results are thought to be theoretically reasonable.

Optimization on the system has been carried out aimed at maximizing the phase fractions of the streams to the compressor and pump respectively. Results have shown an average of less than 5% of dispersed phase in a continuous phase in exit streams.

Preface

This thesis is written as the final work of the Master's of Science in Chemical Engineering at the Norwegian University of Science and Technology (NTNU), 2015.

I would like to extend my sincere thanks to my supervisors Assoc.Prof Johannes J*ä*schke and Prof. Sigurd Skogestad for their technical assistance, support and guidance in this project work.

I would also like to thank Tamal Das for his assistance during the closing stages of this work.

Thank you all.

Declaration of Compliance:
I,Fahad Matovu, hereby declare that this is an independent work according to the exam regulations of the Norwegian University of Science and Technology (NTNU).

Place and date:
Trondheim, Norway;
June 9, 2015

Contents

List of Figures

List of Tables

1 Introduction

Chapter 1 focuses on the general introduction to compact sub-sea separation systems. The reasons behind the emergency of the technology, the motivation and challenges involved, and the objectives of this work.

In chapter 2, a literature review about compact separation systems and the system by Ellingsen (2007) used for this work are introduced. In addition, the functionality of the separators and their parts is covered and some typical applications of compact separators included.

Chapter 3 focuses on the concepts of modelling the separators and the underlying assumptions.

Chapter 4 discusses optimization of the compact separation system including the problem formulation, objective function, constraints, optimization cases and a sensitivity analysis on the optimal solution.

Simulation results of the steady state models and their discussion are presented in the first section of Chapter 5. Optimization and sensitivity analysis results in the second section. Performance in terms of balances on each separator are also presented in table form for the combined separator model and optimal base-case.

The conclusion and future prospects are discussed in chapter 6. All matlab codes used for simulation purposes are attached in the Appendix A.

1.1 Overview

The oil production industry is always faced with a challenge of separating oil well streams into component phases that include oil, water and gas, so as to process them into marketable products or dispose them off in a way that is environmentally friendly (Sayda and Taylor, 2007).

The conventional separation techniques are usually costly, involve equipment of considerable size and weight thereby affecting the space and load requirements, which greatly makes the processing facilities costly (Hamoud et al., 2009). Therefore, efforts are in place to develop technologies for oil processing that reduce the size and weight of process equipment in order to reduce cost and maximise effectiveness. This has led to the emergence of compact inline separation systems.

These systems are interesting prospects as separation technologies for both top-side and sub-sea separation. What makes them interesting is the fact that they minimize space and weight while optimize separation efficiencies and that their application in existing installations has potential to increase production (FMCtechnologies, 2011). The inline technology is also reported to have played a major role in de-bottlenecking and upgrading of existing top-side facilities (Chin et al., 2003),(Hamoud et al., 2009).

In inline separators, the separation is achieved by the use of centrifugal forces that are thousands of times greater than the force of gravity used in conventional separators (Hamoud et al., 2009). In contrast to conventional separators where fluids are allowed to have a few minutes of retention time under the influence of gravity, inline separators need relatively much lesser retention times. This is because the rate of separation is greatly increased in inline separators. The size of the separation vessels is also greatly reduced (Hamoud et al., 2009).

1.2 Motivation for compact separation technology

The reduced size and weight of compact separation technologies are very attractive because of limitation of space and load requirements thus reducing associated capital costs. The reduced weight and space requirements of these systems also help to make marginal fields commercially viable. Compact equipment can also be used in existing installations where space is limited, for debottle-necking (FMCtechnologies, 2011).

Compact equipment can also be used for phase separation for top-side and sub-sea installations because of their reduced size and weight.

Compact equipment are ideal for sub-sea separation and other high pressure applications since pressure vessels can be reduced in size, or sometimes even be eliminated when using inline separation equipment.

Sub-sea separation also results in increased well productivity and accelerated reservoir draining rates. It also reduces the requirement for high efficiency insulation systems especially in risk of formation of hydrates resulting in savings on cost and time required for insulation. Sub-sea separation also results in reduction in size, weight and associated cost of production water treatments installations top-side (Alary et al., 2000).

1.3 Challenges of compact separation technology

However, there are also some potential draw backs. The small residence time associated with the compact separation equipment results in control challenges. The control of liquid and interface levels tends to be more challenging than in conventional separators since the former are more sensitive to flow variations. The reduced size also makes compact separation equipment difficult to operate.

Also, a potential problem with sub-sea separation is the impact of reduced liquid flow rate on flow behaviour which in a line may induce severe slugging. However, solutions to this problem such as the use of gas-lift in the riser exist (Alary et al., 2000). Also limited accessibility and high maintenance costs are challenges to sub-sea separation.

According to Hamoud et al. (2009), the inline separation techniques utilizing centrifugal forces produce outlet streams with quality that is sufficient for practical purposes but may not as good as conventional separators.

1.4 Objectives of this work

The objective of this work is to develop steady state models that can be used to predict the performance of compact separators with a given geometry and known inlet con-

ditions. The performance is in terms of determining the separation efficiency of the dispersed phase in a continuous phase and outlet stream flow rates and phase fractions.

This would then serve as a first step towards developing models for optimization and control of compact sub-sea separators and ultimately compact sub-sea separation systems.

2 Background on Compact Separation Systems

2.1 Literature review

The compact separation technology is a new technology for which information is not readily available about the performance of the cylindrical cyclone separators developed under this technology. A lack of complete understanding of the complex multiphase hydrodynamic flow behaviour inside these separators inhibits complete confidence in their design, performance, application and development. This has therefore hindered the development of holistic models to represent the hydrodynamic flow behaviour inside these separators and the development of suitable simulators.

Nevertheless, some mathematical models have been developed and some experimental investigations carried out. Also, a number of organisations that include FMC technologies, University of Tulsa under the Tulsa University Separation Technology Projects(TUSTP), CDS Engineering BV(Netherlands), Statoil, Eindhoven University of Technology(Mechanical Eng. Dept) and NTNU(Norway) are currently carrying out research in compact separation technologies. Following is a brief overview of some literature.

Bothamley et al. (2013a) part 1 of 3 explores weaknesses and proposes manageable approaches to quantification of feed flow steadiness, entrainment/droplet size distribution, velocity distribution and separator performance of gas/liquid separators with focus on developing a more consistent approach to sizing. Part 2 discusses methods for improved quantification of operational performance and part 3 presents results of selected case studies to show the effects of key sizing decision parameters, fluid properties and operational parameters.

Kouba and Shoham (1996), is a review paper that discusses the status of development of some form of compact cylindrical cyclone called the Gas liquid cylindrical cyclone

(GLCC), some aspects of its modelling, and current installations and potential applications. Mechanistic models of compact cylindrical cyclones of different forms have been developed, improved or discussed by (Arpandi, 1995), (Kouba et al., 1995),(Arpandi et al., 1996), (Marti et al., 1996),(Gomez et al., 2000), (van Wissen et al., 2007),(Monsen, 2012) and (Stene, 2013).

Arpandi (1995) developed a mechanistic model for the prediction of hydrodynamic behaviour of two-phase flow in GLCC separators. The model predicts flow variables such as equilibrium liquid level, gas-liquid interface shape, zero-net liquid flow holdup, onset of liquid carry-over by annular mist flow, operational envelope for liquid carry-over, bubble trajectory, as well as liquid holdup, velocity distributions and total pressure drop across the GLCC. The developed model was extended by Marti et al. (1996) for predicting the onset of gas carry-under and bubble separation efficiency. Gomez et al. (2000) enhanced the model by incorporating a flow pattern dependent nozzle analysis of the cylindrical cyclone inlet for prediction of the gas and liquid tangential velocities at the GLCC entrance. The proposed model was used to design four typical field GLCC systems for actual industrial applications.

van Wissen et al. (2007) discussed a comparison between a rotating particle separator (RPS) and axial cyclone for ultra fine particle removal of contaminants such as CO_2, H_2S from natural gas. The RPS is an axial cyclone where the rotating element contained in a cylindrical stationary pipe consists of a multitude of axially oriented channels. The comparison parameters were residence time, specific energy consumption and volume flow. In conclusion, the RPS was shown to be able to separate an order of magnitude smaller particles than the axial cyclone at equal residence time, specific energy consumption and volume flow. The energy consumption was an order of magnitude less for the RPS than the cyclone at the same droplet diameter and the through-put was higher.

Pereyra et al. (2009) presented a dynamic model and simulator for prediction of flow behaviour under transient slugging flow conditions that were developed for the Gas-Liquid Cylindrical Cyclone/Slug Damper (GLCC-SD) system. Separate dynamic models and simulators were developed for each unit and integrated into an overall model/simulator for the system. Simulation results presented demonstrate the advantage of the system in

dampening and smoothing liquid flow rate under slug flow conditions. It is reported by Pereyra et al. (2009) that the simulator developed can be extended to other separators such as the gravity separators and liquid hydrocyclones.

Monsen (2012) studied one-dimensional models describing pressure drop and separation performance of the NTNU Natural Gas Liquid Separator (NNGLseparator) for dispersed gas-liquid flows. The modelling of separation performance was divided into droplet capture by the meshpad followed by cyclonic separation and then combined in sequence. To model this separation mechanism, a modified time of flight model was developed. The modification includes the mesh porosity, and a β-factor describing the droplets' reduced radial velocity due to the obstructing meshpad. The proposed one-dimensional models were then analysed through a parametric study of the separator performance in terms of pressure drop and efficiency of droplet separation for different flow conditions and geometries.

Stene (2013) used Computational Fluid Dynamics (CFD) tools to study a rotating gas liquid separator (Lynx separator) developed at NTNU. This is a vertical separator with a rotating aluminium mesh pad. Simulations were performed in ANSYS FLUENT using a Turbulent k-ω model in combination with Discrete Phase Model.

Experimental studies have also been carried out on the performance of compact separators and there are some field applications currently. For example, Movafaghian et al. (2000) studied experimentally and theoretically the hydrodynamic flow behaviour in a GLCC (Gas liquid cylindrical cyclone) compact separator. New experimental data comprising of equilibrium liquid level, zero-net liquid flow holdup and the operational envelope for liquid carry-over were obtained using a 7.62 cm I.D, 2.18 m high, GLCC separator for a wide range of operating conditions. The data was utilized to verify and refine an existing GLCC mechanistic model in which case the comparison between the modified model predictions and the experimental data showed a very good agreement.

The article by Chin et al. (2003) focuses on the design and installation of an inline deliquidizer where design, laboratory and field results are presented. The article also highlights that during laboratory and offshore tests, the inline deliquidizer was shown

to remove 90-95%+ of the liquid upstream of the vessel. Also, Schook et al. (2005) describes inline separators based on inline technology and their application on different platforms forexample Statfjord-B degasser and BP-Etap deliquidizer applications, along with their specific benefits and cost savings.

The concepts, objectives and benefits of inline separation technology application in a Saudi Arabia wet gas field are discussed by Hamoud et al. (2009). The article concludes by reporting that the technology has been recognized to optimize gas well production and de-bottleneck existing facilities facing capacity limitation. Also, the technology is anticipated to reduce capital and operating costs for future oil and gas field developments.

The literature above discusses units that use concepts of centrifugal separation but their geometry in most cases and modelling interests are quite different from the units of our interest. Hence, it is only some ideas that have been taken up in this work.

2.2 Compact separation system by Ellingsen

The compact separation system used for this work is that according to Ellingsen (2007) as shown in figure 2.1 below.

As seen from figure 2.1, there are three separation units. Some of the units discussed here are based on a new-inline technology where a centrifugal force is used to separate the phases because of their difference in densities. This separation system is compact because the units minimise space and weight and are designed to have almost the same dimensions as the transport pipe thus inline-technology (Ellingsen, 2007).

The gravity separator does the bulk separation of the gas and liquid phases that enter the unit. However, the separation obtained is not satisfactory as regards the demands of the compressor and pump. Therefore, the degasser and deliquidizer do further separation of the phases. The degasser separates gas from a liquid dominated stream while the deliquidizer separates liquid from a gas dominated stream (FMCtechnologies, 2011).

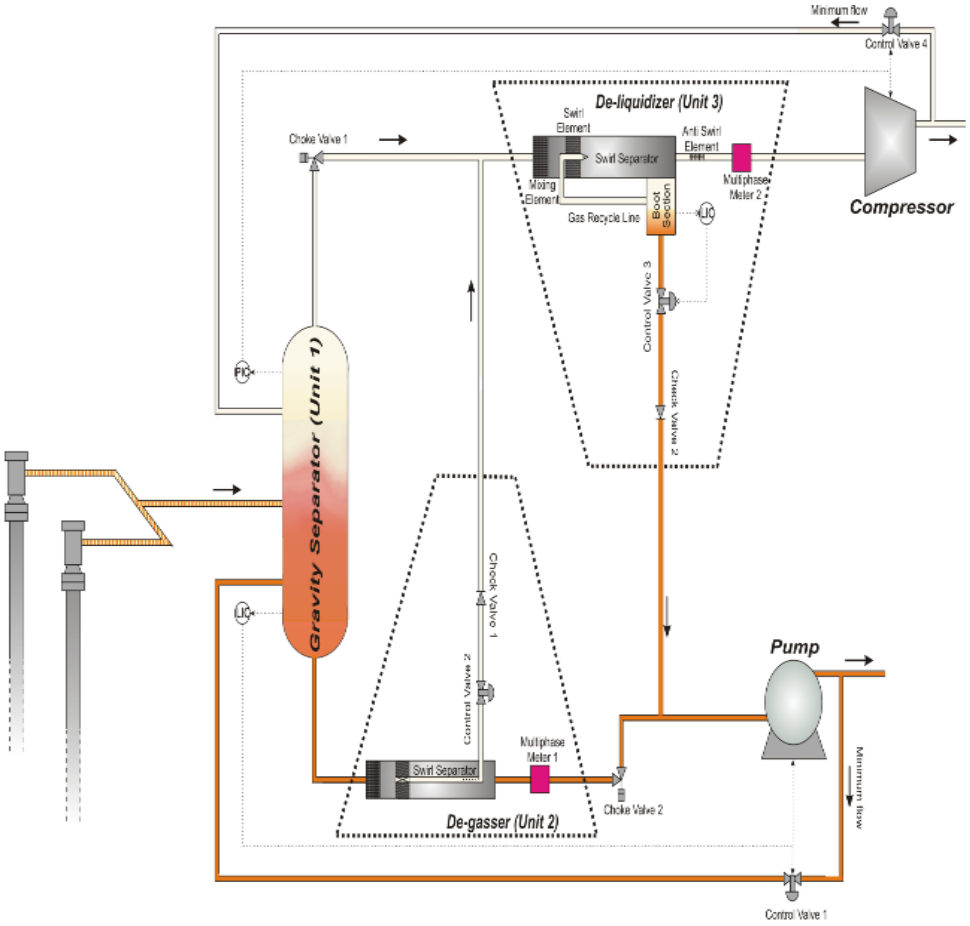

Figure 2.1: Compact separation system by Ellingsen
Adapted from (Ellingsen, 2007)

It is important to note about the compact separation system in figure 2.1 that the operational objective is to adjust the available valves in such a way that the gas content in the liquid stream to the pump is minimised. Therefore the quality of the liquid from the degasser is more important than the gas quality and therefore the gas phase from the degasser undergoes further separation in the deliquidizer.

Note that the return streams of liquid and gas after the pump and compressor are not meant for use under normal operation. They are meant to ensure that there is enough feed to the pump and compressor and that the flow rates through the deliquidizer and degasser are above certain limits (Ellingsen, 2007).

2.3 Gravity separators

These are pressure vessels that separate a mixed stream of liquid and gas phases into respective separate phases (Mokhatab and Poe, 2012). They employ the use of the gravity forces to separate the mixed phases based on their differences in density. The heavier phase settles at the bottom of the separator while the lightest rises to the top but this requires some settling time. The larger the difference in density, the higher the difference in velocity resulting in a lower settling time.

However, for large settling times, the separators need to be larger to effect the separation. Due to the fact that large separator vessel sizes are required to achieve settling, gravity separators are rarely designed to remove droplets smaller than 250 μm (Mokhatab and Poe, 2012).

Gravity separators are often classified to be vertical or horizontal based on their geometrical configuration or by their function. For example,they are “two-phase” if they separate gas from a liquid stream (Mokhatab and Poe, 2012).

The figure 2.2 below is that of a vertical two phase separator for oil and gas.

The two-phase mixture enters the separator through the feed pipe into the inlet device. The main function of this device is to improve separation efficiency by maximization of

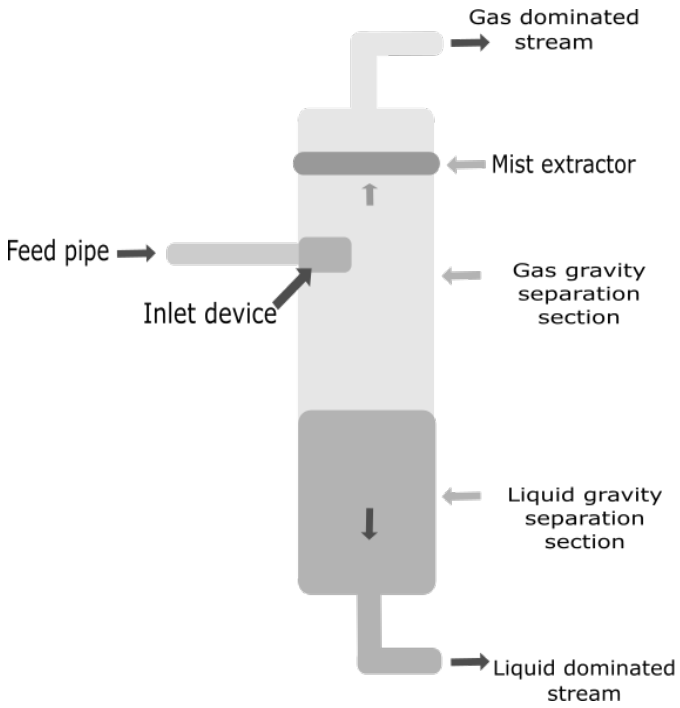

Figure 2.2: Vertical gas liquid separator

gas/liquid separation efficiency, minimization of droplet shearing and provision of good downstream velocity distributions of separated phases (Bothamley et al., 2013a).

In the gas gravity separation section, the entrained liquid load is reduced by separation of liquid droplets from the gas phase. The mist extractor in addition is used to remove liquid droplets remaining at the outlet of the gas gravity separation section.

On the other hand, free gas is separated out of the liquid in the liquid gravity separation section (Bothamley et al., 2013b).

The separated gas and liquid phases exit at the top and bottom respectively.

2.4 Deliquidizer

The deliqudizer is one of the units in the separation system discussed that is compact and based on the inline technology. The role of the deliquidizer is to separate liquid

from the gas dominated stream from the gravity separator where bulk separation takes place. The components of a typical deliquidizer are shown in the figure 2.3 below.

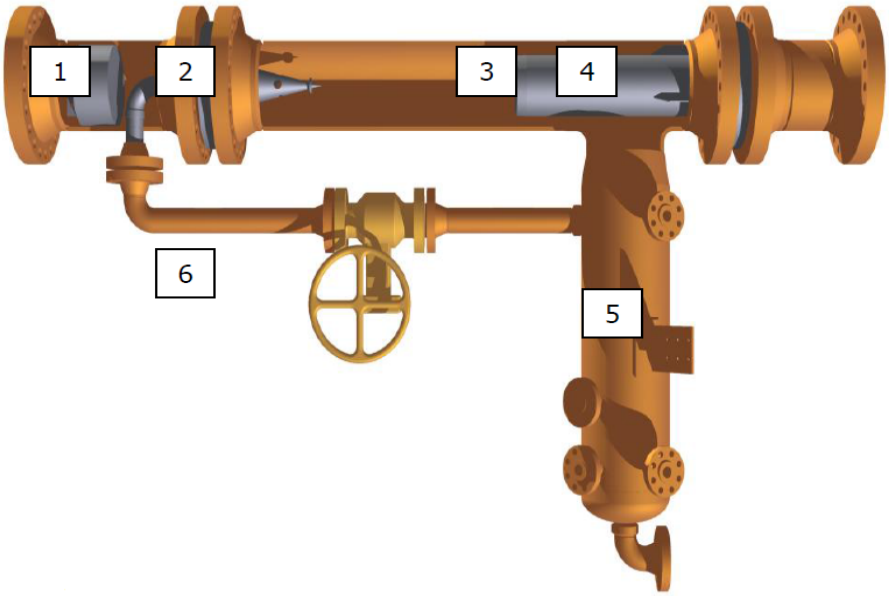

Figure 2.3: Typical inline deliquidizer
Adapted from (FMCtechnologies)

The multiphase flow stream enters the unit through a flow conditioning element(1) which equally distributes the liquid droplets throughout the pipe cross sectional area. The stationary swirl element(2) then brings the two phase mixture into rotation which causes the two phases to separate because of their difference in densities. The liquid creates a thin film on the pipe's outer wall and the gas exits through a small pipe in the center of the main pipe(3) (Hamoud et al., 2009). The liquid enters the annular space between the two pipes, hits the back wall of the deliquidizer and enters the boot scetion(5). This liquid carries some gas and the latter is removed and recycled back through the recycle line(6). The liquid is discharged at the bottom of the boot section. The gas outlet pipe(4) has an anti-swirl element which stops the rotation, resulting in a low-total pressure drop across the deliquidizer. The control of the deliquidizer will only require level control for the liquid from the boot section (Hamoud et al., 2009).

A successful deliquidizer installation as seen in figure 2.4 was implemented on the BP-ETAP platform in the North sea in May 2003 (Schook et al., 2005). The ETAP deliquidizer, a $20''$ unit was installed to reduce the amount of condensate that is eventually carried by the HP gas cooler discharge drum to the downstream Glycol contactor, so as to achieve the required water dew point of the export gas. The condensate caused problems for the Glycol contactor and Glycol regeneration unit resulting in financial losses as a result of glycol losses and filter replacements.

Figure 2.4: BP ETAP deliquidizer installed on a platform in the North sea
Adapted from (Schook et al., 2005)

2.5 Degasser

The role of the degasser in the compact separation system here discussed is to separate gas from the liquid stream from the gravity separator after bulk separation. This is also a compact unit based on the inline technology.

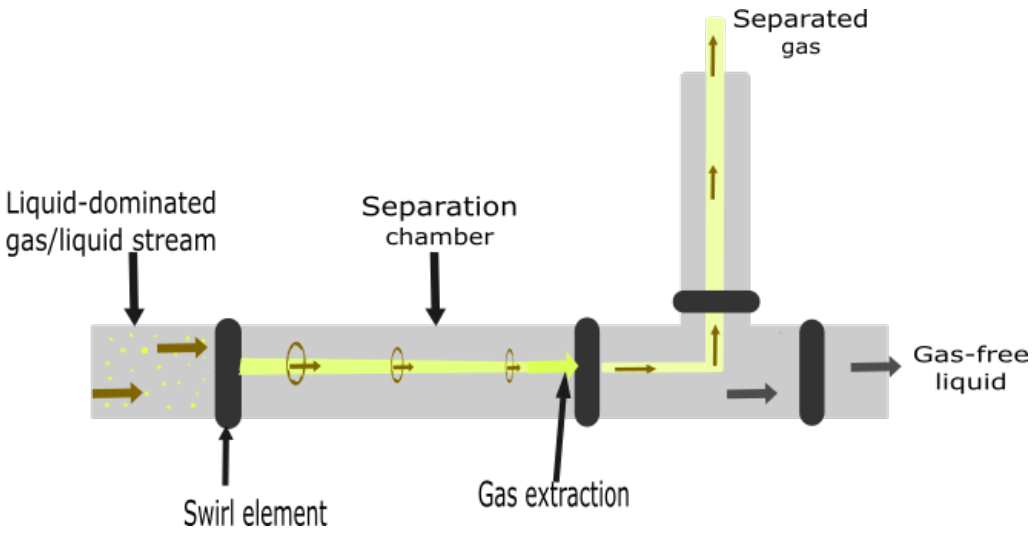

Figure 2.5: Typical inline degasser

As can be seen from figure 2.5, the liquid dominated gas liquid stream in this case from the gravity separator enters the unit and is forced into rotation by the swirl element near the entrance. The rotation of the mixture stream enhances separation of the phases with the gas core forming in the centre of the unit (FMCtechnologies, 2011). The gas core then enters the smaller diameter pipe in the centre of the degasser and is discharged to the deliquidizer while the gas free-liquid continues to the exit of the unit and to the pump.

A typical degasser installation as seen in figure 2.6 was implemented on the Statoil Statfjord-B platform in September 2003. The installation was to reduce the amount of gas in the produced water line where high volumetric gas fractions (about 30%) resulted in slug flow powerful vibrations and flare instability that caused safety and environmental problems (Schook et al., 2005). The operation was successful and resulted in very dry gas separated from the water, vanishing of all vibrations in produced water line and a stable flare system.

Figure 2.6: Degasser installed at the test site and off-shore on Statfjord-B platform
Adapted from (Schook et al., 2005)

3 Modelling of Compact Separation System Units

3.1 Modelling of the gravity separator

The nomenclature for the gravity separator to be used in the model equations is as shown in the figure 3.1 below.

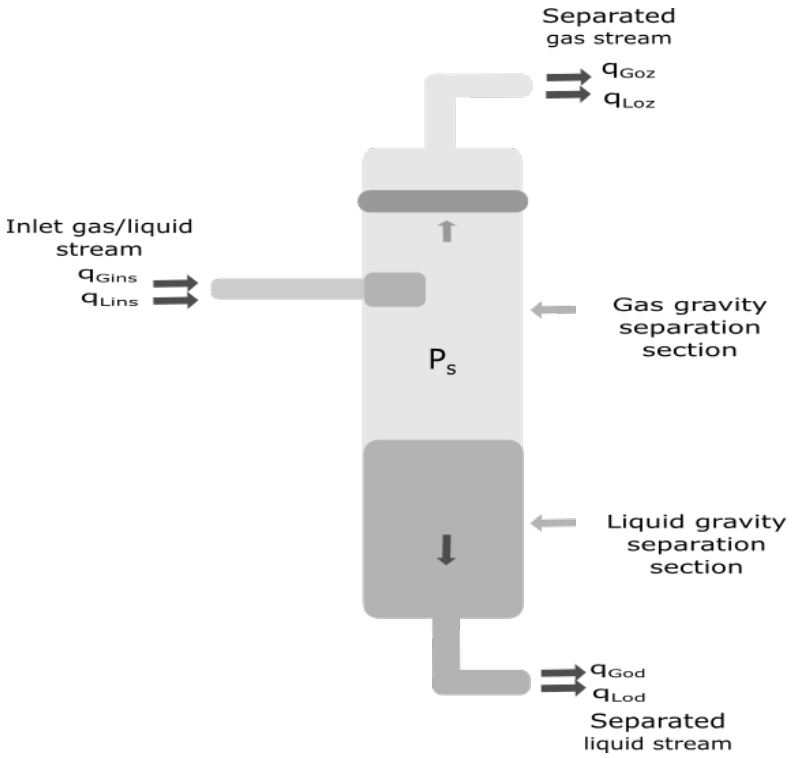

Figure 3.1: Nomenclature of gravity separator for modelling

The description of the variables used in model equations is shown in table 3.1 below.

The overall liquid balance gives;

Table 3.1: Description of variables for gravity separator modelling

Variable	Description	Unit
q_{Gins}	Inlet gas flow rate	m^3/s
q_{Lins}	Inlet liquid flow rate	m^3/s
q_{Goz}	Outlet gas flow rate to deliquidizer	m^3/s
q_{Loz}	Outlet liquid flow rate to deliquidizer	m^3/s
q_{God}	Outlet gas flow rate to degasser	m^3/s
q_{Lod}	Outlet liquid flow rate to degasser	m^3/s
P_s	Pressure in separator	Pa

$$\frac{dm_L}{dt} = \dot{m}_{Lins} - \dot{m}_{Loz} - \dot{m}_{Lod} \tag{3.1}$$

where $\dot{m}_L = \rho_L q_L$ and for incompressible liquid flow, this gives;

$$\frac{dV_L}{dt} = q_{Lins} - q_{Loz} - q_{Lod} \tag{3.2}$$

where V_L is volume of liquid in the gravity separator.

The overall gas balance gives;

$$\frac{dm_G}{dt} = \dot{m}_{Ginz} - \dot{m}_{Goz} - \dot{m}_{God} \tag{3.3}$$

Therefore,

$$\frac{dm_G}{dt} = \rho_G(q_{Gins} - q_{Goz} - q_{God}) \tag{3.4}$$

Differentiating the gas equation of state, $P_s V_G = Z\bar{R}T m_G$ yields;

$$V_G \frac{dP_s}{dt} = Z\bar{R}T \frac{dm_G}{dt} - P_s \frac{dV_G}{dt} \tag{3.5}$$

where $\bar{R} = R/M_G$ and R and M_G are the universal gas constant and gas molecular weight respectively. For an overall volume balance, $\frac{dV_L}{dt} = -\frac{dV_G}{dt}$ and thus equation 3.5 becomes;

$$V_G \frac{dP_s}{dt} = Z\bar{R}T \frac{dm_G}{dt} + P_s \frac{dV_L}{dt} \tag{3.6}$$

For $\rho_G = \frac{P_s}{Z\bar{R}T}$, substituting equations 3.2, 3.4 into equation 3.6 gives;

$$V_G \frac{dP_s}{dt} = P_s(q_{Gins} - q_{Goz} - q_{God} + (q_{Lins} - q_{Loz} - q_{Lod})) \tag{3.7}$$

3.1.1 Entrainment in feed pipe

There are a variety of factors that are important in sizing and performance prediction of most types of separation equipment such as the flow pattern at the separator inlet, amount of dispersed phase present in entrained form and sizes of the droplets/bubbles. However, there quantification is difficult and typically requires simplifying assumptions (Bothamley et al., 2013a).

The flow pattern at the inlet is generally dependent on the relative amounts of gas and liquid in the feed pipe and in-situ phase velocities (Bothamley et al., 2013a) but this analysis is not considered further in this report. The focus is rather on the other factors. We assume that the inlet flow pattern is in such a way that the phase velocities are sufficiently large enough for dispersion of the phases to take place.

The amount of liquid entrainment as droplets in the gas significantly affects the separation between the phases and increases with increasing gas velocities and decreasing liquid surface tension (Bothamley et al., 2013a).

The liquid droplet entrainment has been predicted using a correlation developed for annular flow by Pan and Hanratty (2002) but is also applicable to non-annular (lower velocity) flows (Bothamley et al., 2013a). This correlation also includes a method of estimating the Sauter-mean diameter (d_{32}) of the entrained liquid droplet size distribution as shown in equation 3.8 below.

$$\begin{aligned} \frac{(E/E_m)}{1-(E/E_m)} &= 9e-08\left(\frac{Du_g^3\sqrt{\rho_l\rho_g}}{\sigma}\right)\left(\frac{\rho_g^{1-m}\mu_g^m}{d_{32}^{1+m}g\rho_l}\right)^{\frac{1}{(2-m)}} \\ \left(\frac{\rho_g u_g^2 d_{32}}{\sigma}\right)\left(\frac{d_{32}}{D}\right) &= 0.0091, \end{aligned} \tag{3.8}$$

The description of the variables and parameters in equation 3.8 is shown in the table 3.2 below. (Note that the factor $9e-08$ in equation 3.8 has in the simulations been replaced by 9 so as to achieve higher entrainment fractions. This is done to ensure that we have poorer phase separation than was originally predicted.)

Table 3.2: Description of variables for the Entrainment correlation

Variable	Description	Unit
E	Entrainment fraction	$-$
E_m	Maximum entrainment fraction	$-$
D	Pipe inside diameter	m
u_g	Gas velocity	m/s
ρ_g	Gas density	kg/m^3
ρ_l	Liquid density	kg/m^3
σ	Liquid surface tension	N/m
μ_g	Gas viscosity	$kg/m.s$
g	Acceleration due to gravity	m/s^2
d_{32}	Sauter-mean diameter	m
m	Settling law exponent	$-$

3.1.2 Droplet sizes and distributions

There are a number of correlations that have been developed to predict droplet sizes of entrained liquid and most of the work has been focused on annular flow conditions (Bothamley et al., 2013a). Nevertheless, we assume that they apply to our flow conditions and the volume median diameter (d_{v50}) is estimated as given by Kataoka et al. (1983), Bothamley et al. (2013a).

By definition, the volume median diameter (d_{v50}) is the value where 50% of the total volume of droplets is made up of droplets with diameters larger than the median value and the rest smaller. The maximum droplet size is said to be in range 3-5 times d_{v50} (Bothamley et al., 2013a).

The volume median diameter is given by;

$$\begin{aligned} d_{v50} &= 0.01(\frac{\sigma}{\rho_g u_g^2})Re_g^{2/3}(\frac{\rho_g}{\rho_l})^{-1/3}(\frac{\mu_g}{\mu_l})^{2/3} \\ Re_g &= \frac{Du_g\rho_g}{\mu_g}, \end{aligned} \tag{3.9}$$

where μ_l is liquid viscosity and Re_g is gas phase Reynolds number.

A look at equation 3.9 shows that the volume median diameter d_{v50} decreases with increasing gas velocity, increasing gas density and decreasing surface tension.

Upper-Limit Log Normal distribution

The Upper-limit log normal distribution has been used by Simmons and Hanratty (2001), Bothamley et al. (2013a) to represent droplets of entrained liquid in two-phase flow.

The normalized volume frequency distribution is given as follows;

$$
\begin{aligned}
f_v(d_p) &= \frac{\delta d_{max}}{\sqrt{\pi} d_p (d_{max} - d_p)} exp(-\delta^2 z^2) \\
&\textit{where} \\
z &= \ln\left(\frac{a d_p}{d_{max} - d_p}\right) \\
a &= \frac{d_{max} - d_{v50}}{d_{v50}} \\
\delta &= \frac{0.394}{\log\left(\frac{v_{90}}{v_{50}}\right)} \\
v_i &= \frac{d_i}{d_{max} - d_i}
\end{aligned}
\tag{3.10}
$$

As is seen from equation 3.10, the distribution function is characterised by parameters d_{max}, d_{v50} and δ.

Typical values of a, δ and d_{max} used are $a = 4.0$, $\delta = 0.72$ and $d_{max} = 5.0\,d_{v50}$ as given by Bothamley et al. (2013a).

The Cumulative volume distribution is obtained by integration of the volume frequency distribution (equation 3.10) and is given as;

$$V_{under} = 1 - 0.5(1 - erf(\delta z)) \tag{3.11}$$

where erf(x) is the error function (Bothamley et al., 2013a).

The figure 3.2 shows a typical plot of Normalized and Cumulative volume distributions for the entrained liquid (Entrainment fraction $E = 0.0603$).

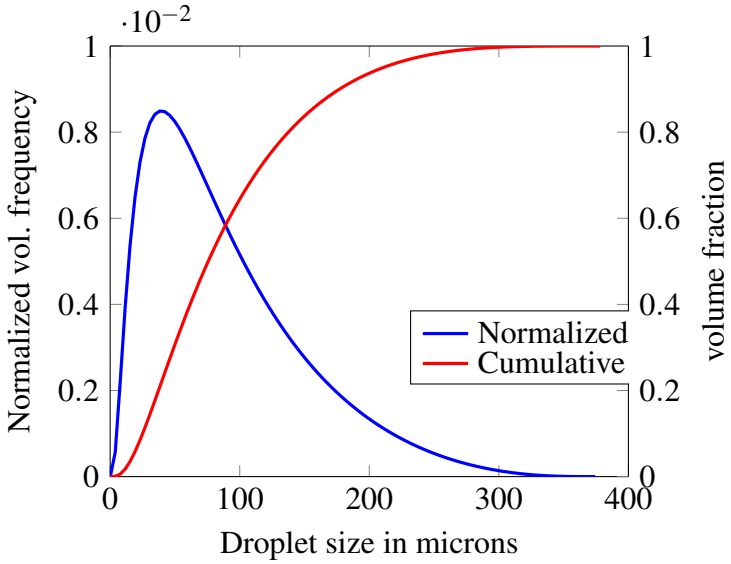

Figure 3.2: Normalized and Cumulative volume distributions of entrained liquid Entrainment fraction $E = 0.0603$, $a = 4.0$, $\delta = 0.72$ and $d_{max} = 5.0\,d_{v50} = 378$

3.1.3 Separation in gas gravity section

A drag force is exerted on the liquid droplets entrained in the gas phase. For the separation of the liquid droplets to take place, the external force applied on the droplets must exceed the drag force. The most basic force applied is the gravitational force . For the droplet to separate, the gravitational force minus the bouyancy force must equal the drag force (Monsen, 2012). Therefore a force balance gives,

$$(\rho_l - \rho_g) g V_p = F_D \tag{3.12}$$

where ρ_l is the density of the liquid, ρ_g is the density of the gas, V_p is the volume of the droplet, g is the gravitation constant and F_D is the drag force.

The drag force F_D is based on stoke's law, considering the droplet to be spherical and of a small diameter (Stene, 2013). Then,

$$F_D = 3\pi U_t d_p \mu_g = 6\pi U_t r_p \mu_g \tag{3.13}$$

where U_t is the droplet terminal velocity, d_p and r_p are the droplet diameter and radius respectively, μ_g is the gas viscosity. Therefore substituting for F_D in equation 3.12 gives,

$$(\rho_l - \rho_g)gV_p = 6\pi U_t r_p \mu_g \tag{3.14}$$

Substituting for $V_p = \frac{4}{3}\pi r_p^3$ in equation 3.14 and making U_t the subject gives,

$$U_t = \frac{2(\rho_l - \rho_g)gr_p^2}{9\mu_g} \tag{3.15}$$

Therefore;

$$U_t = \frac{(\rho_l - \rho_g)gd_p^2}{18\mu_g} \tag{3.16}$$

The above terminal velocity equation represents the stable velocity the droplet reaches after an acceleration period in gas flow. The dependance of the terminal velocity on the droplet diameter results in the fact that smaller droplets attain their terminal velocity after a short time period than larger droplets (Stene, 2013).

The velocity profile of a continuous phase (gas, oil,or water) in a separator has historically been calculated from $V = Q/A$ where Q is the in-situ volumetric flow rate of the continuous phase and A is the cross-sectional area for flow (Bothamley et al., 2013a).

Therefore the gas velocity is given by;

$$u_g = \frac{4Q_g}{\pi D^2} \tag{3.17}$$

where Q_g is gas volumetric flow rate and D is the diameter of the gravity separator.

Therefore the terminal velocity of droplets U_t must be greater than or equal to the gas velocity u_g for the droplets to be separated from the gas phase.

For $U_t = u_g$, it is possible to determine the "critical droplet size" dp_{crit} of the droplet distribution above which all droplets are separated from the gas flow.

$$dp_{crit} = \left(\frac{72 Q_g \mu_g}{\pi D^2 (\rho_l - \rho_g) g} \right)^{1/2} \tag{3.18}$$

From the cumulative volume distribution as given by equation 3.11, the volume fraction of entrained liquid that remains in the gas flow is given by;

$$\beta_{carry-over} = 1 - 0.5(1 - erf(\delta z_{crit})) \tag{3.19}$$

where $z_{crit} = \ln(\frac{a dp_{crit}}{d_{max} - dp_{crit}})$.

Therefore, the separation efficiency of the entrained liquid is given by;

$$\eta_{eff} = 1 - \beta_{carry-over} \tag{3.20}$$

3.1.4 Gas and liquid volume fractions of exit streams

The gas volume fraction of the exiting gas stream at the top of the gravity separator is given by;

$$\alpha_g = \frac{q_{Goz}}{q_{Toz}} = \frac{q_{Goz}}{q_{Goz} + q_{Loz}} \tag{3.21}$$

where q_{Toz} is the total outlet flow rate to deliquidizer.

Note; $q_{Loz} = q_{Lins} E \beta_{carry-over}$ where E is the liquid entrainment fraction.

The liquid volume fraction of the exiting stream at the bottom of the gravity separator is given by;

$$\beta_l = \frac{q_{Lod}}{q_{Tod}} = \frac{q_{Lod}}{q_{Lod} + q_{God}} \tag{3.22}$$

where $q_{Lod} = q_{Lins} - q_{Loz}$.

We note that the terms q_{Goz} and q_{God} are unknown.

Analogous to the analysis for the liquid dispersed in gas as has been discussed above, we assume that gas is also dispersed into the liquid and behaves in a similar manner and thus summarise the behaviour as follows;

The gas entrainment is predicted by;

$$\begin{aligned} \frac{(Eg/E_m)}{1-(Eg/E_m)} &= 9\left(\frac{Du_l^3\sqrt{\rho_l\rho_g}}{\sigma}\right)\left(\frac{\rho_l^{1-m}\mu_l^m}{d_{32g}^{1+m}g\rho_l}\right)^{\frac{1}{(2-m)}} \\ \left(\frac{\rho_l u_l^2 d_{32g}}{\sigma}\right)\left(\frac{d_{32g}}{D}\right) &= 0.0091, \end{aligned} \tag{3.23}$$

The volume median diameter of the bubble size distribution (d_{v50g})is given by;

$$\begin{aligned} d_{v50g} &= 0.01\left(\frac{\sigma}{\rho_l u_l^2}\right)Re_l^{2/3}\left(\frac{\rho_l}{\rho_g}\right)^{-1/3}\left(\frac{\mu_l}{\mu_g}\right)^{2/3} \\ Re_l &= \frac{Du_l\rho_l}{\mu_l}, \end{aligned} \tag{3.24}$$

The bubble rise velocity is given by an equation similar to that of the droplet terminal velocity (equation 3.16) as given below;

Therefore;

$$U_r = \frac{(\rho_l-\rho_g)gd_p^2}{18\mu_l} \tag{3.25}$$

The liquid velocity is also given by;

$$u_l = \frac{4Q_l}{\pi D^2} \tag{3.26}$$

where Q_l is liquid volumetric flow rate and D is the diameter of the gravity separator.

Therefore the bubble rise velocity U_r must be greater than or equal to the liquid velocity u_l for the bubbles to be separated from the liquid phase.

For $U_r = u_l$, the "critical bubble size" dp_{critg} of the bubble size distribution above which all bubbles are large enough to be separated from the liquid is given by;

$$dp_{critg} = \left(\frac{72 Q_l \mu_l}{\pi D^2 (\rho_l - \rho_g) g} \right)^{1/2} \tag{3.27}$$

From the cumulative volume distribution as given by equation 3.11, the volume fraction of entrained gas that remains in the liquid flow is given by;

$$\beta_{carry-under} = 1 - 0.5(1 - erf(\delta z_{critg})) \tag{3.28}$$

where $z_{critg} = \ln(\frac{ad p_{critg}}{d_{maxg} - dp_{critg}})$ and $d_{maxg} = 5 d_{v50g}$.

Therefore, the separation efficiency of the entrained gas is given by;

$$\eta_{effg} = 1 - \beta_{carry-under} \tag{3.29}$$

Therefore, the amount of gas carried with the liquid stream exiting at the bottom of the gravity separator is given by;

$$q_{God} = q_{Gins} Eg \beta_{carry-under} \tag{3.30}$$

where Eg is the gas entrainment fraction.

Thus; $q_{Goz} = q_{Gins} - q_{God}$. Therefore, the phase fractions as defined by equations 3.21 and 3.22 can be determined.

3.2 Modelling of the Deliquidizer

It's important to state that some of the concepts used for modelling in the following sections are normally applied in particle technology but have been assumed to apply here as well.

The interest here is the separation of liquid droplets from an inlet gas dominated stream and thus predict the outlet gas and liquid volume fractions and flow rates at the top and bottom of the deliquidzier.

The nomenclature to be used is as shown in the figure 3.3 below.

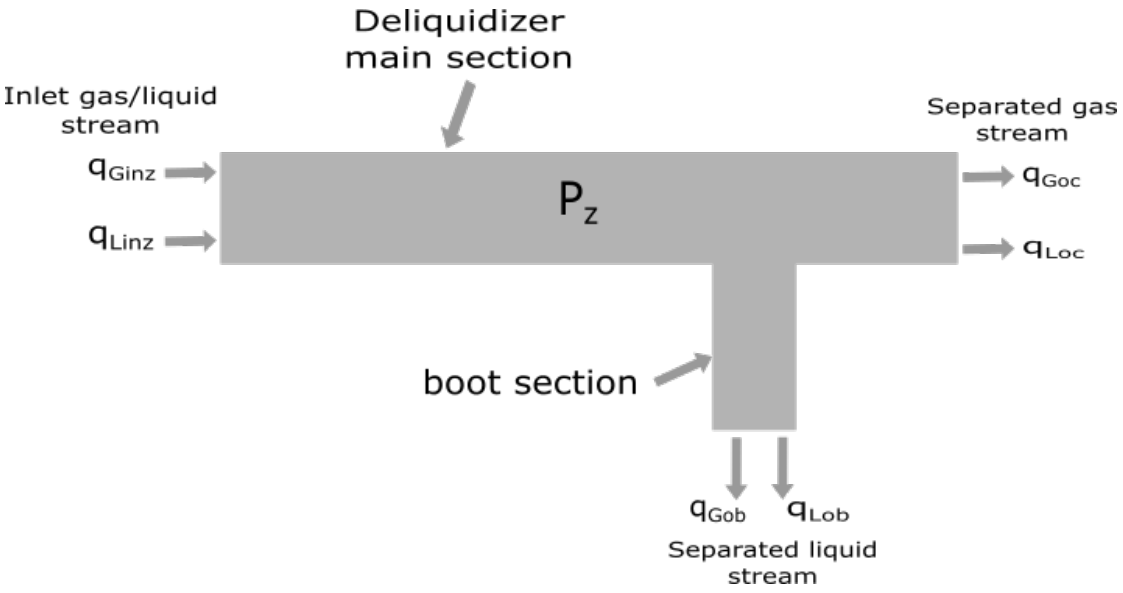

Figure 3.3: Nomenclature of deliquidizer for modelling

The description of the variables used in model equations is shown in table 3.3 below.

The overall liquid balance gives;

$$\frac{dm_L}{dt} = \dot{m}_{Linz} - \dot{m}_{Loc} - \dot{m}_{Lob} \tag{3.31}$$

where $\dot{m}_L = \rho_L q_L$ and for incompressible liquid flow, this gives;

Table 3.3: Description of variables for deliquidizer modelling

Variable	Description	Unit
q_{Ginz}	Inlet gas flow rate	m^3/s
q_{Linz}	Inlet liquid flow rate	m^3/s
q_{Goc}	Outlet gas flow rate to compressor	m^3/s
q_{Loc}	Outlet liquid flow rate to compressor	m^3/s
q_{Gob}	Outlet gas flow rate from boot section	m^3/s
q_{Lob}	Outlet liquid flow rate from boot section	m^3/s
P_z	Pressure in deliquidizer	Pa

$$\frac{dV_L}{dt} = q_{Linz} - q_{Loc} - q_{Lob} \tag{3.32}$$

where V_L is volume of liquid in deliquidizer.

At steady state, this gives;

$$q_{Linz} = q_{Loc} + q_{Lob} \tag{3.33}$$

The overall gas balance gives;

$$\frac{dm_G}{dt} = \dot{m}_{Ginz} - \dot{m}_{Goc} - \dot{m}_{Gob} \tag{3.34}$$

Therefore,

$$\frac{dm_G}{dt} = \rho_G(q_{Ginz} - q_{Goc} - q_{Gob}) \tag{3.35}$$

Assuming steady state conditions and that the gas density is constant, this gives;

$$q_{Ginz} = q_{Goc} + q_{Gob} \tag{3.36}$$

3.2.1 Cyclonic separation in the deliquidizer

In this subsection, modelling of cyclonic separation is considered where the forces present push the heavier liquid phase outwards to the wall while the lighter gas phase remains in the middle section. The external forces (centrifugal forces) generated in this case are greater than the gravitational forces used in conventional separators and therefore retention times for phase separation are greatly reduced.

Radial velocity

A look at equation 3.15 shows that the external force involved is the gravitational force. However, for cyclonic separation, there are centrifugal forces, thus the centripetal acceleration a_c which is assumed to have a greater influence on the droplet than gravity replaces the gravitational acceleration g in the above equation (Stene, 2013). The centripetal acceleration a_c is given by $a_c = \frac{u_t^2}{r}$ where u_t is the tangential velocity and r the radial position.

In a cylindrical geometry, equation 3.15 can now be written as;

$$u_r = \frac{dr}{dt} = \frac{(\rho_l - \rho_g) d_p^2 u_t^2}{18 \mu_g r} \tag{3.37}$$

The swirl flow in the deliquidizer is assumed to be a forced vortex flow, which is swirling flow with the same tangential velocity distribution as a rotating solid body as opposed to free vortex flow, the way a frictionless fluid would swirl. This is done for simplicity as the tangential velocity distribution for real swirling flows is intermediate between these two extreme cases (Hoffmann and Stein, 2002). In addition, Swanborn (1988) shows that the tangential velocity distribution at the inlet is close to a forced vortex and perhaps our assumption is not as bad since we consider conditions at the inlet but the validity of this assumption has not been justified.

For a forced vortex flow, the tangential velocity u_t is given by $u_t = \omega r$ where ω is the angular velocity measured in radians per unit of time and is a constant for a forced

vortex flow (Hoffmann and Stein, 2002). Substituting for u_t in equation 3.37 gives

$$u_r = \frac{dr}{dt} = \frac{(\rho_l - \rho_g) d_p^2 \omega^2 r}{18 \mu_g} \tag{3.38}$$

Time of flight model

The time of flight model is a comparison of the time required by the droplet that enters at a certain inlet position to reach the cyclone wall to the time available to traverse the length of the cyclone (Hoffmann and Stein, 2002).

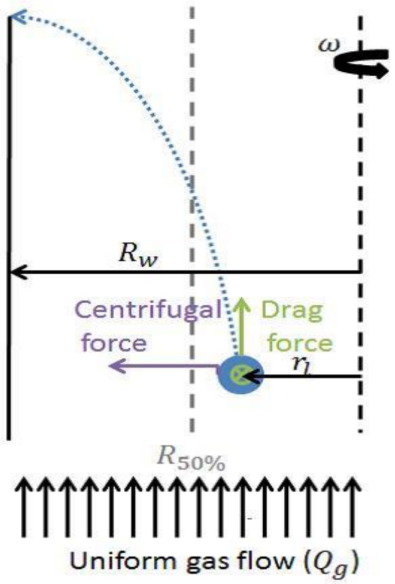

Figure 3.4: Trajectory of droplet experiencing a centrifugal force
Adapted from (Monsen, 2012)

Figure 3.4 illustrates how the radial velocity affects the droplet trajectory. The gas entrained with liquid droplets enters the separator and is set into circular motion. The centrifugal and drag forces cause the radial velocity of the droplet to increase resulting in an arced trajectory (Monsen, 2012).

Assuming that a droplet enters at an inlet position r_l, where r_l is the distance from

the its inlet position to the separator centre, the time t_{radial} for the droplet to reach the separator wall R can be obtained by integration of equation 3.38 from r_l to R (Monsen, 2012). This gives;

$$t_{radial} = \frac{18\mu_g}{(\rho_l - \rho_g)d_p^2\omega^2} \ln \frac{R}{r_l} \tag{3.39}$$

On the other hand, the time t_{axial} available for the droplet from the inlet to exit of the separator is given by;

$$t_{axial} = \frac{L}{v_z} = \frac{\pi R^2 L}{q_{Tinz}} \tag{3.40}$$

where L is the length of the separator, v_z is the axial velocity and q_{Tinz} is the total inlet volumetric flow rate.

A comparison of t_{radial} and t_{axial} leads to possible cases. Either t_{radial} is less than t_{axial}, implying that the liquid droplet will reach the wall before exiting the separator thus separating from gas flow. Or t_{radial} is greater than t_{axial}, implying that the liquid droplet will not reach the wall of the separator and remains entrained in the gas flow (Monsen, 2012).

Based on this analysis, it's possible to find the "critical droplet entrance position" r_l above which all the liquid droplets are separated if they are of the same diameter d_p and are uniformly distributed across the cross-sectional area of the separator, if the diameter d_p and the angular velocity ω are known or can be estimated. This position is shown in figure 3.5 below.

Therefore, equating the two expressions for t_{radial} and t_{axial}, it is possible to find the position r_l. Thus;

$$\frac{18\mu_g}{(\rho_l - \rho_g)d_p^2\omega^2} \ln \frac{R}{r_l} = \frac{\pi R^2 L}{q_{Tinz}} \tag{3.41}$$

Making r_l the subject gives;

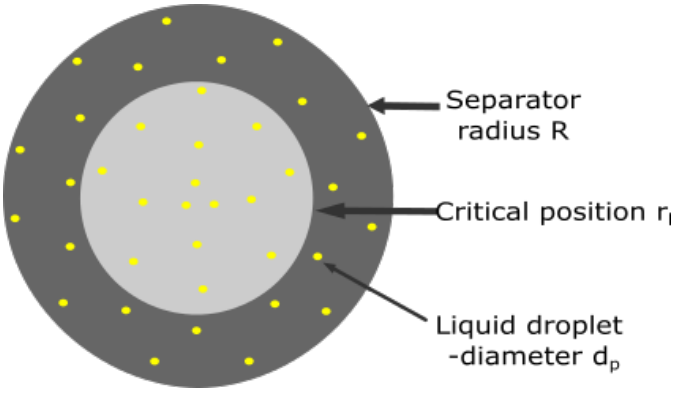

Figure 3.5: Theoretical cross sectional view of the critical droplet entrance position r_l for separation

$$r_l = \exp(\ln R - \frac{(\rho_l - \rho_g) d_p^2 \omega^2 \pi R^2 L}{18 \mu_g q_{Tinz}}) \tag{3.42}$$

$$r_l = \exp(\ln R - \frac{(\rho_l - \rho_g) d_p^2 \omega^2 t_{axial}}{18 \mu_g}) \tag{3.43}$$

It's quite obvious from equation 3.42 that r_l is dependent on the inlet volumetric flow rate q_{Tinz}, angular velocity ω, droplet diameter d_p, density difference between the phases to be separated $\rho_l - \rho_g$, viscosity of the continuous phase μ_g and the length L and radius R of the separator.

Uniform droplet distribution

It's assumed in this model that all the liquid is dispersed into droplets of a certain size, diameter d_p that are distributed uniformly into the gas phase. This assumption is supported by the fact that there is a mixing element at the start of the deliquidizer whose role is to equally distribute the liquid droplets throughout the pipe cross sectional area.

Let n be the total number of droplets entering the unit. The number of droplets per unit cross sectional area $n_a = \frac{n}{\pi R^2}$. The number of droplets separated n_{sep} (with t_{radial}

less than t_{axial}) are in the cross sectional area $\pi(R^2 - r_l^2)$. Thus $n_{sep} = n_a\pi(R^2 - r_l^2) = n(1 - (\frac{r_l}{R})^2)$.

Therefore, volume separated $V_{sep} = n(1 - (\frac{r_l}{R})^2)V_p$ where $V_p = \frac{4}{3}\pi r_p^3$ is the volume of each droplet. But nV_p is the total volume of liquid into the separator. Therefore the volumetric flow rate of liquid separated $\dot{V}_{sep} = q_{Linz}(1 - (\frac{r_l}{R})^2)$ where q_{Linz} is the volumetric flow rate of liquid into the separator. If q_{Tinz} is the total inlet volumetric flow rate and f is the gas volume fraction, then $q_{Linz} = (1 - f)q_{Tinz}$. Therefore, $\dot{V}_{sep}$ is given by;

$$\dot{V}_{sep} = (1 - f)q_{Tinz}(1 - (\frac{r_l}{R})^2) \tag{3.44}$$

The equation 3.44 predicts the volumetric flow rate of liquid separated from the gas phase in the deliquidizer. Note that r_l is dependent on other parameters as previously discussed in this subsection. Therefore, the volumetric flow rate of liquid separated $\dot{V}_{sep}$ is similarly dependent on the same parameters.

On the other hand, a closer look at figure 3.5 shows that the liquid separation efficiency can be determined, thus;

$$\eta_{eff} = \frac{Area\,above\,r_l}{Cross\,sectional\,area} = \frac{R^2 - r_l^2}{R^2} \tag{3.45}$$

Phase fractions of exit streams

Finally, the gas volume fraction α_g of the exiting stream after separation of the liquid is given by;

$$\alpha_g = \frac{q_{Toc} - q_{Loc}}{q_{Toc}} \tag{3.46}$$

where $q_{Toc} = q_{Goc} + q_{Loc}$

The top flow rate $q_{Toc} = F * q_{Tinz}$ where F is the split fraction and q_{Tinz} is the total inlet flow rate and both F and q_{Tinz} are assumed to be known.

Assuming that all the separated liquid exits the deliquidizer through the bottom, then $q_{Lob} = \dot{V}_{sep}$ and $q_{Loc} = q_{Linz} - q_{Lob}$. Thus α_g can be determined.

We have not considered separation in the boot section of the deliquidizer and thus assume that all the gas and liquid that does not leave through the top outlet stream exits through the bottom stream. Therefore, the liquid volume fraction β_l of the bottom stream is given by;

$$\beta_l = \frac{q_{Lob}}{q_{Lob} + q_{Gob}} \tag{3.47}$$

Effective swirl

The concept of “Effective swirl" in this case has been used to represent a variation of angular velocity ω with inlet volumetric flow rate and its definition does not stand for the term “swirl" as applied in fluid dynamics.

The representation of this concept for the purposes of this report is a Gompertz function of the form (ref Wikipedia);

$$y(t) = a * exp(-b * exp(-c * t)) \tag{3.48}$$

where a is an asymptote, b sets the displacement along the x-axis and c sets the growth rate(y scaling). b and c are positive numbers. This is a sigmoid function where growth is slowest at the start and end of the independent variable. Therefore, the angular velocity as a function of the inlet volumetric flow rate is represented as given by equation 3.49 below.

$$\omega = a * exp(-b * exp(-c * q_{Tinz})) \tag{3.49}$$

This representation of the angular velocity as a Gompertz function was used in the model and predictions obtained were compared to data.

The representation of angular velocity as a simple power function of the volumetric flow rate was also tried for comparison purposes to determine which of the functions best represented the angular velocity. The Gompertz function representation produced better predictions and is further used in this report.

The lsqcurvefit in Matlab was used to find parameters a,b,c for the gompertz function that best fit the model outlet gas volume fraction predictions to experimental data (This experimental data is found in *mod_deliq* in Appendix A.1).

Model improvement to cater for phase mix-up after separation

The concept of droplet breakup at high Reynold's numbers was used to improve the model. According to Van Campen (2014), the acceleration of a dispersed liquid-liquid system can lead to droplet breakup. Droplets exist due to interfacial tension force and forces acting on the interface, such as shear and viscous forces cause droplet deformation. If these forces exceed the interfacial tension force by a critical extent, the droplet breaks into two or more smaller droplets.

Even though Van Campen (2014) discusses liquid-liquid systems, we have used the idea of droplet breakup for a gas-liquid system. He further states that Hinze (1955) proposed a model for the maximum droplet size in turbulent flow as follows;

$$D_{max}(\frac{\rho_c}{\sigma})^{3/5}\varepsilon^{2/5} = 0.725 \tag{3.50}$$

where ρ_c is the density of the continuous phase, σ is the interfacial tension and ε the turbulent dissipation rate. The turbulent length scale can be estimated by;

$$l = (\frac{v^3}{\varepsilon})^{1/4} = l_o Re^{-3/4} \tag{3.51}$$

where v is the kinematic viscosity and l_o the scale of the largest eddy (the tube diameter). The turbulent kinetic energy can then be expressed as;

$$\varepsilon = \frac{v^3 Re^3}{l_o^4} = \frac{u^3}{D} \tag{3.52}$$

where u is average velocity and D is tube diameter.

Also, $u = \frac{4q_{Tinz}}{\pi D^2}$ where q_{Tinz} is the volumetric flow rate. Substituting for ε in equation 3.50 gives;

$$D_{max} = 0.725(\frac{\sigma}{\rho_c})^{3/5}(\frac{\pi^3 D^7}{64 q_{Tinz}^3})^{2/5} \tag{3.53}$$

The equation 3.53 show a relationship between the droplet size D_{max} and volumetric flow rate q_{Tinz}. For the case of simplicity, an inverse linear relationship of the form $D_{max} = mq_{Tinz} + c$ with m and c being the slope and intercept respectively was used for improvement of model predictions. The parameters m and c were determined by validation of the model predictions against experimental data.

3.3 Modelling of the Degasser

The modelling interest for this separator is the separation of gas bubbles from an inlet liquid dominated stream and thus predict the gas and liquid volume fractions and flow rates of the exiting streams.

The nomenclature to be used is as shown in the figure 3.6 below.

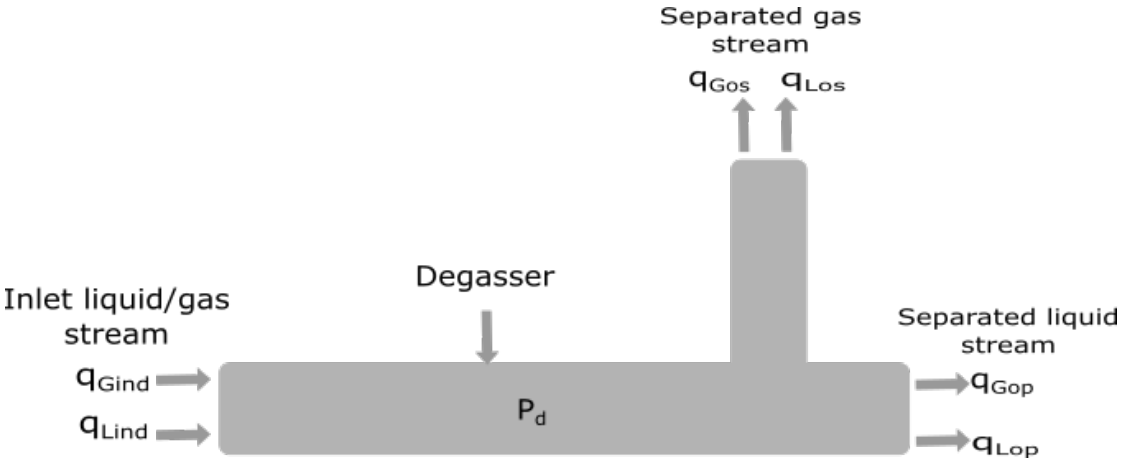

Figure 3.6: Nomenclature of degasser for modelling

The description of the variables used in model equations is shown in table 3.4 below.

Table 3.4: Description of variables for degasser modelling

Variable	Description	Unit
q_{Gind}	Inlet gas flow rate	m^3/s
q_{Lind}	Inlet liquid flow rate	m^3/s
q_{Gop}	Outlet gas flow rate to pump	m^3/s
q_{Lop}	Outlet liquid flow rate to pump	m^3/s
q_{Gos}	Outlet gas flow rate to deliquidizer	m^3/s
q_{Los}	Outlet liquid flow rate to deliquidizer	m^3/s
P_d	Pressure in degasser	Pa

The overall liquid balance gives;

$$\frac{dm_{Ld}}{dt} = \dot{m}_{Lind} - \dot{m}_{Los} - \dot{m}_{Lop} \tag{3.54}$$

where $\dot{m}_{Ld} = \rho_L q_L$ and for incompressible liquid flow, this gives;

$$\frac{dV_{Ld}}{dt} = q_{Lind} - q_{Los} - q_{Lop} \tag{3.55}$$

where V_{Ld} is volume of liquid in degasser.

At steady state, we obtain;

$$q_{Lind} = q_{Los} + q_{Lop} \tag{3.56}$$

The overall gas balance gives;

$$\frac{dm_{Gd}}{dt} = \dot{m}_{Gind} - \dot{m}_{Gos} - \dot{m}_{Gop} \tag{3.57}$$

Therefore,

$$\frac{dm_{Gd}}{dt} = \rho_G(q_{Gind} - q_{Gos} - q_{Gop}) \tag{3.58}$$

Assuming steady state conditions and that the gas density is constant, we obtain;

$$q_{Gind} = q_{Gos} + q_{Gop} \tag{3.59}$$

3.3.1 Cyclonic separation in the degasser

The approach used in this case is similar to that as was used for the deliquidizer. However, we now have gas bubbles dispersed in a liquid stream which are separated to form a gas core in the centre of the degasser. The forces that apply are similar as was discussed in subsection 3.2.1.

We therefore consider the radial velocity of the gas bubbles experiencing centripetal acceleration as given by;

$$u_r = \frac{dr}{dt} = \frac{(\rho_g - \rho_l) d_p^2 u_t^2}{18 \mu_l r} \tag{3.60}$$

where u_t is the tangential velocity.

The vortex associated with cyclonic separation is a combined vortex with a forced vortex in the central region and a free vortex on the outside of the region (Monsen, 2012). However, we once again consider the vortex to be a forced vortex and therefore the tangential velocity is given as follows.

$$u_t = 2\pi r \omega \tag{3.61}$$

where ω is the angular frequency.

Let us consider a gas bubble entering the separator at radial position $r = r_{in}$, the radial time it takes to reach the gas pipe radius $r = r_{pp}$ is given by substitution of 3.61 into 3.60 and integration yields;

$$t_{radial} = \frac{18 \mu_l}{4\pi^2 (\rho_g - \rho_l) d_p^2 \omega^2} \ln \frac{r_{pp}}{r_{in}} \tag{3.62}$$

On the other hand, the time t_{axial} available for the bubble from the inlet to exit of the separator is given by;

$$t_{axial} = \frac{L}{u_z} = \frac{\pi R^2 L}{q_{Tind}} \tag{3.63}$$

where L is the length of the separator, u_z is the axial velocity and q_{Tind} is the total inlet volumetric flow rate.

A comparison of t_{radial} and t_{axial} leads to possible cases. Either t_{radial} is less than t_{axial}, implying that the gas bubble will be separated. Or t_{radial} is greater than t_{axial}, implying that the gas bubble will not reach the gas core in the separator centre and remains entrained in the liquid.

Therefore it's possible to find the "critical bubble entrance position" r_l below which all the gas bubbles are separated if they are of the same diameter d_p and are uniformly distributed across the cross-sectional area of the separator. This gives;

$$\frac{18\mu_l}{4\pi^2(\rho_g-\rho_l)d_p^2\omega^2}\ln\frac{r_{pp}}{r_l}=\frac{\pi R^2 L}{q_{Tind}} \tag{3.64}$$

Making r_l the subject gives;

$$r_l=\exp(\ln r_{pp}-\frac{4\pi^2(\rho_g-\rho_l)d_p^2\omega^2\pi R^2 L}{18\mu_l q_{Tind}}) \tag{3.65}$$

Therefore;

$$r_l=r_{pp}\exp(-\frac{4\pi^2(\rho_g-\rho_l)d_p^2\omega^2 t_{axial}}{18\mu_l}) \tag{3.66}$$

Uniform droplet distribution and separation efficiency

Assuming that the gas phase is uniformly dispersed into bubbles of a certain size, diameter d_p that are distributed uniformly over the entire cross sectional area. Figure 3.7 below shows a cross-sectional view of the "critical bubble entrance position r_l".

We assume that all the gas bubbles below the "critical bubble entrance position r_l" are separated. Thus the separation efficiency η of the degasser is predicted as follows;

$$\eta=\frac{\pi(r_l^2-r_{pp}^2)}{\pi(R^2-r_{pp}^2)} \tag{3.67}$$

The flow rate of separated gas q_{gsep} is obtained as a product of gas flow rate into the degasser and separation efficiency, thus;

$$q_{gsep}=q_{Gind}\frac{(r_l^2-r_{pp}^2)}{(R^2-r_{pp}^2)} \tag{3.68}$$

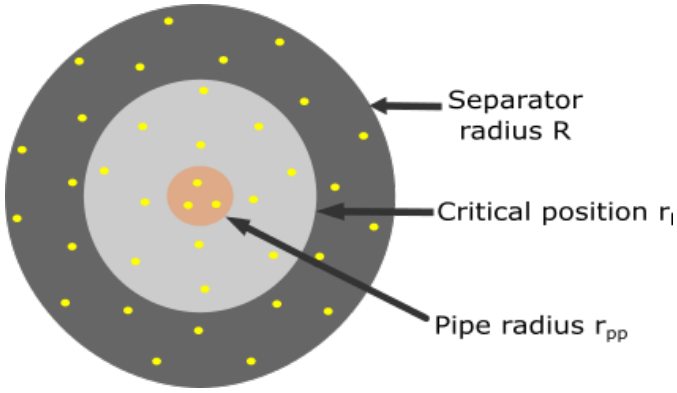

Figure 3.7: Theoretical cross-sectional view of "critical bubble entrance position r_l" for separation

If the liquid volume fraction of the inlet stream is β, then $q_{Gind} = (1-\beta)q_{Tind}$. Therefore,

$$q_{gsep} = (1-\beta)q_{Tind}\frac{(r_l^2 - r_{pp}^2)}{(R^2 - r_{pp}^2)} \tag{3.69}$$

Phase fractions of exiting streams

The top flow rate $q_{Tos} = F * q_{Tind}$ where F is the split fraction and q_{Tind} is the total inlet flow rate and both F and q_{Tind} are assumed to be known.

There are two cases that can arise for the determination of liquid top flow rate to the deliquidizer q_{Los}. Either $q_{gsep} \geq q_{Tos}$ implying that the gas stream to the deliquidizer is pure gas. It does not carry any liquid with it and therefore $q_{Los} = 0$. Alternatively, $q_{gsep} < q_{Tos}$ implying that the stream to the deliquidizer has both gas and liquid phases. Therefore,

$$q_{Los} = \begin{cases} q_{Tos} - q_{gsep}, & \text{if } q_{gsep} < q_{Tos}. \\ 0, & \text{if } q_{gsep} \geq q_{Tos}\ . \end{cases} \tag{3.70}$$

However, for now we assume that all the separated gas exits the degasser through the

top stream, then $q_{Gos} = q_{gsep}$ and $q_{Los} = q_{Tos} - q_{Gos}$.

The gas volume fraction α_g of the top exiting stream can be determined as follows;

$$\alpha_g = \frac{q_{Gos}}{q_{Tos}} \tag{3.71}$$

Finally, the liquid volume fraction β_l of the exiting bottom stream to the pump, after separation of the gas is given by;

$$\beta_l = \frac{q_{Lop}}{q_{Tind} - q_{Tos}} \tag{3.72}$$

where $q_{Lop} = q_{Lind} - q_{Los}$

4 Optimization

The main reason for focusing on optimization is the consideration of the performance of a process. The goal of an optimization problem is to minimize an objective function J subject to given equality and inequality constraints g and h respectively. Therefore, a steady state optimization problem can be formulated as follows (Rangaiah and Kariwala, 2012);

$$\begin{aligned} & min_u J(u,x,d) \\ & \text{subject to constraints:} \\ & g(u,x,d) = 0 \\ & h(u,x,d) \leq 0 \end{aligned} \tag{4.1}$$

where u, x and d are steady state degrees of freedom, states and disturbances respectively. g represents equality constraints that include model equations which relate the independent variables (u and d) to the states(x) and h represents inequality constraints (such as non-negative flows, volume fractions less or equal to 1). Therefore the system must satisfy the given inequality constraints. In most cases, some subset h' of the inequality constraints h are active ($h' = 0$ at the optimal solution). These active constraints are satisfied by adjusting a corresponding number of degrees of freedom (Skogestad, 2004).

4.1 Problem formulation

Th figure 4.1 below shows the compact separation system for optimization. All variables corresponding to a given stream shall be denoted by the respective stream number for example q_{g1}, f_1 denote the volumetric flow rate and gas volume fraction of stream 1.

The manipulated variables are assumed to be the split fractions (F1 and F2) on the degasser and deliquidizer respectively. These are fractions of the total inlet flow rates and set the total outlet flow rates of the top streams exiting the degasser and deliquidizer.

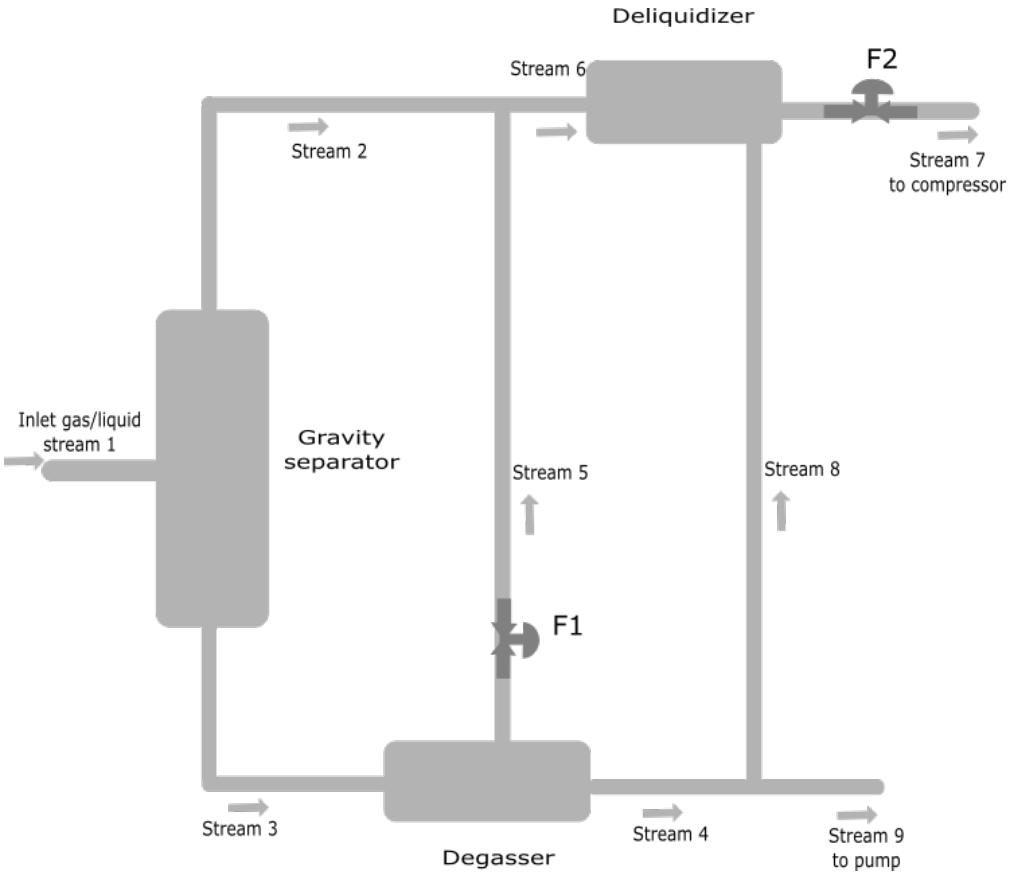

Figure 4.1: Nomenclature of compact separation system for optimization

We assume that there is no degree of freedom on the gravity separator since the model as described in section 3.1 fixes the output flow rates and phase fractions for a fixed inlet flow rate and gas volume fraction if other parameters are kept constant. The disturbance variables are assumed to be the volumetric flow rate and phase fraction of the gas/liquid stream to the gravity separator (stream 1). The output variables are the flow rates and phase fractions (f and β being gas and liquid volume fractions) of streams exiting the separators.

The objective here is to have an acceptable (near-optimal) operation of the system with the maximum achievable gas and liquid volume fractions of the streams exiting to the compressor and pump respectively. This translates to the minimization of the amounts of liquid in the gas stream to the compressor and gas in the liquid stream to the pump.

The presence of a condensate or water in a gas to the compressor results in a reduction in compressor performance, compressor corrosion and increases the mechanical stress on the impellers due to an increased mass flow rate (Brenne et al., 2008). Therefore, it's advantageous from an economical point of view to reduce this liquid amount to a minimum. In addition, the presence of gas in liquid to the pump is also considered detrimental to the performance and life of a pump and therefore this amount of gas should also be minimized.

4.2 Objective function

We wish to maximize the average of gas and liquid volume fractions of streams 7 and 9 respectively. The optimization has been done in Matlab using $fmincon$ as the solver and since Matlab optimization solvers handle only minimization problems, the maximization problem is defined as negative function. Thus, the objective function J is as follows;

$$J(F1,F2) = -0.5(f_7 + \beta_9) \tag{4.2}$$

where f_7 and β_9 are gas and liquid fractions of streams 7 and 9 to the compressor and pump respectively. They are also functions of $F1$ and $F2$. The 0.5 in equation 4.2 is to take an average of phase fractions $f_7$and β_9 so that the objective function value also lies between 0 and 1.

A combination of the models of the three separation units gives a complete model for the compact separation system. The complete model outputs are phase fractions f_7,β_9 and flow rates q_7, q_{g7}, q_{l7}, q_9, q_{g9} and q_{l9}.

4.3 Constraints

The constraints used are linear and non-linear inequality constraints. The linear inequality constraints are posed from the split fractions which are the available degrees of freedom. The split fractions $F1$ and $F2$ are defined as $F1 = \frac{q_5}{q_3}$ and $F2 = \frac{q_7}{q_6}$ and thus we assume that $0 \leq F1, F2 \leq 1$. This gives 4 linear inequality constraints of the form $A.x \leq b$ where $x = [F1, F2]^\intercal$

$$A = \begin{bmatrix} 1 & 0 \\ -1 & 0 \\ 0 & 1 \\ 0 & -1 \end{bmatrix} \tag{4.3}$$

and

$$b = [1, 0, 1, 0]^\intercal \tag{4.4}$$

The non-linear inequality constraints are derived from the fact that the gas and liquid volume fractions are less or equal to 1 and the flow rates should be non-negative. Thus [f_2, f_5, f_6, f_7, β_3 and $\beta_4 \leq 1$] and [q_{g3}, q_{l5} and $q_{g8} \geq 0$]. The choice to constraint only these three flow streams might not be clear to the reader but has been based on experience with the developed models that they in some few cases are susceptible to having these as negative flows. Writing the non-linear inequality constraints in the form $C(x) \leq 0$ gives;

$$C = [f_2 - 1, f_5 - 1, f_6 - 1, f_7 - 1, \beta_3 - 1, \beta_4 - 1, -q_{g3}, -q_{l5}, -q_{g8}]^{\mathsf{T}} \tag{4.5}$$

4.4 Optimization cases

The table 4.1 shows the five different optimization cases that were considered.

Table 4.1: Optimization cases

Cases	Inlet gas fraction f_1	Inlet flow rate q_1, m^3/h
Base case	0.65	150
Case2	0.65	157.5
Case3	0.65	142.5
Case4	0.715	150
Case5	0.585	150

The base case is used to determine the optimal variables and the other cases are considered for evaluating the influence of the inlet gas fraction and inlet flow rate on the optimal performance. Cases 2 and 3 represent $\pm 5\%$ changes in inlet flow rate q_1 and cases 4 and 5 represent $\pm 10\%$ changes in inlet gas fraction f_1 respectively.

4.5 Sensitivity analysis

It is possible that the optimal value of a process variable is unaffected by certain parameters (low sensitivity) in which case it's not very necessary to determine precise values of these parameters for finding the true optimum (Edgar et al., 1989) or vice-versa. This effect of the parameters on the optimum has been computed by calculating the relative sensitivities as given by Edgar et al. (1989). The relative sensitivity for C^{opt} to parameter P is given by;

$$S_P^C = \frac{\partial C^{opt}/C^{opt}}{\partial P/P} \tag{4.6}$$

where C is the objective function value and optimization variables $F1$ and $F2$ and P are parameters q_1 and f_1.

The optimization results are shown and discussed in section 5.2.

5 Results and discussion

All results presented in this chapter are generated in Matlab by implementation of the models developed in the previous chapters. All the necessary Matlab codes are attached in Appendix A.

The parameters as shown in the table 5.1 have been used to obtain the results to be presented in the next sections with a few exceptions and are attached in the Appendix A.1 as a Matlab function *par_css.m*.

Table 5.1: Parameters used to obtain model results

Parameter	Description	Value	Unit
ρ_g	Gas density	15.7	kg/m^3
ρ_l	Liquid density	850	kg/m^3
μ_g	Gas viscosity	1.83e-05	$kg/m.s$
μ_l	Liquid viscosity	16.7e-03	$kg/m.s$
D	Inlet pipe diameter	0.1	m
D_g	Diameter gravity separator	1	m
g	Acceleration due to gravity	9.81	m/s^2
E_m	Maximum entrainment fraction	0.99	–
m	Settling law exponent	1	–
σ	Liquid surface tension	0.032	N/m
R	Radius of degasser	9e-02	m
r_g	Radius of gas extraction pipe	$R\sqrt{0.18}$	m
L_2	Length of degasser	2	m
R_3	Radius of deliquidizer	7.5e-02	m
L_3	Length of deliquidizer	1.5	m

5.1 Model results

5.1.1 Gravity separator

The Matlab code for this separator mod_grav.m is attached to Appendix A.1.2. The figure 5.1 below shows the model results obtained for inlet gas fractions of 0.7 and 0.5. It is seen from the figure that Entrainment fractions of each dispersed phase in a continuous one increase with increasing inlet flow rate because increased flow rates result in increased velocities thus phase dispersion increases, resulting into higher entrainment fractions.

In addition, the separation efficiencies also decrease with increasing flow rates. For example, for the liquid phase, as the inlet flow rate increases, the gas velocity increases outweighing the liquid terminal velocity. This liquid is thus carried with the top gas stream resulting in lower gas volume fractions of the top outlet stream. Also as the liquid separation efficiency decreases, more liquid remains entrained in the gas stream resulting in lower gas fractions.

A similar scenario occurs for the gas phase in which case an increase in inlet flow rates results in higher liquid velocities. Thus the gas rise velocities become smaller in comparison to liquid velocities and more gas is carried by the outlet bottom stream resulting in lower separation efficiencies and lower liquid volume fractions.

The above arguments are in agreement with the analysis and results by Bothamley et al. (2013a), who reports that higher inlet momentum rates (higher feed pipe velocities) result in higher entrainment loads, smaller droplet sizes and more difficult separation conditions.

It can also been seen from the model predictions in figure 5.1 that a decrease of the inlet gas volume fraction from 0.7 to 0.5 for the same conditions results in an decrease in liquid entrainment and higher liquid separation efficiency. However, gas entrainment in liquid increases resulting in lower gas separation efficiency and therefore the top stream gas volume fraction decreases. In addition the bottom stream liquid volume fraction

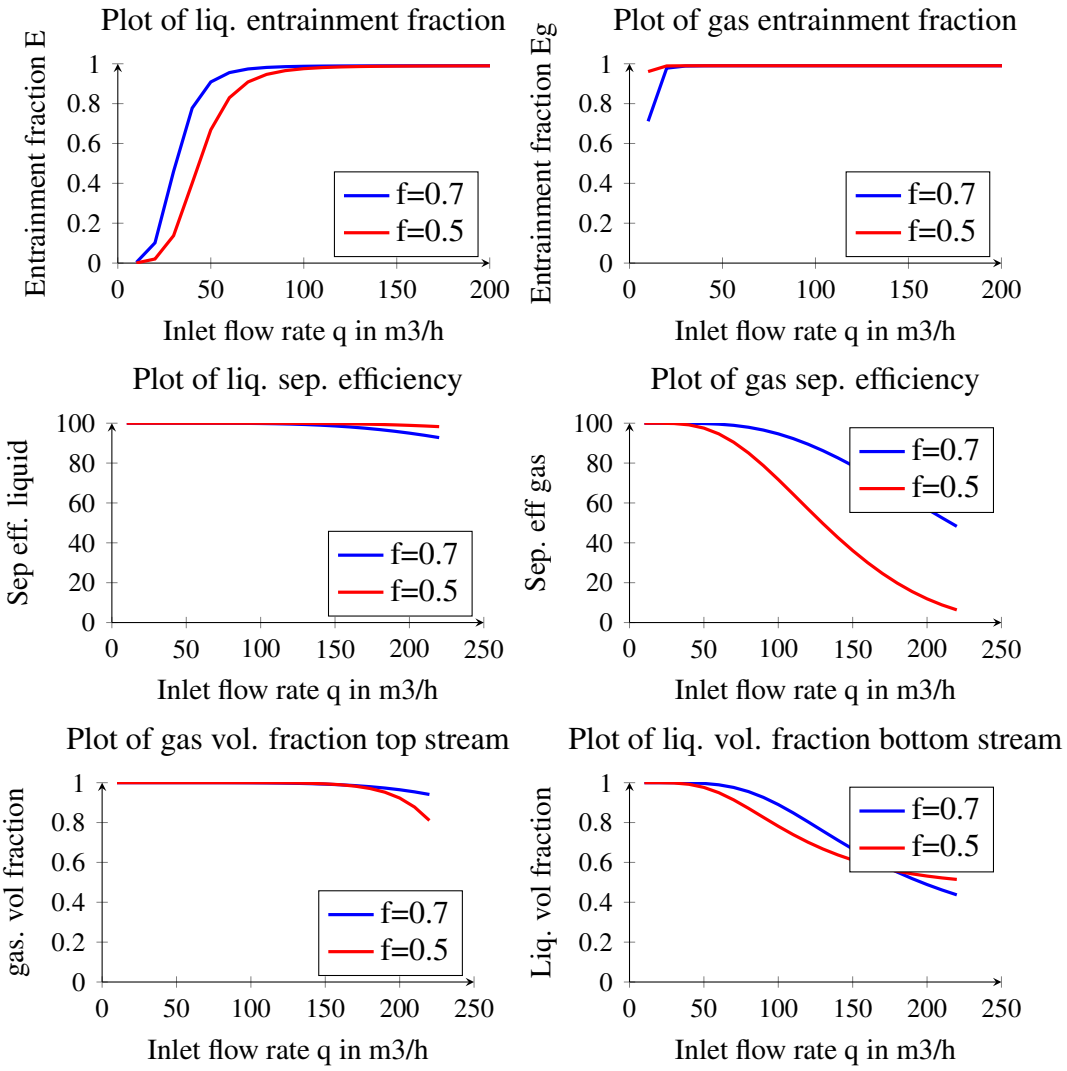

Figure 5.1: Gravity separator performance for Inlet stream gas fractions f=0.7 & 0.5 The subplots 1 to 6 represent plots for liquid and gas entrainment fractions, liquid and gas separation efficiencies, top stream gas and bottom stream liquid fractions respectively.

also decreases because of increased gas content.

5.1.2 Deliquidizer

The Matlab code for this separator mod_deliq.m is attached to Appendix A.1.3. The results obtained for this separator are shown in figure 5.2 below.

At low inlet flow rates, the swirl intensities generated are low resulting in low angular velocities and low radial velocities. This results in low centrifugal forces which are desired for phase separation and hence low liquid separation efficiencies.

An increase in inlet flow rate results in increased angular velocities and ultimately increased separation forces. Therefore, the liquid separation efficiency increases. This decreases the amount of liquid in the gas stream thus the gas volume fraction of the top stream also increases as shown in sub-plot 3. Also, since more liquid is separated, the amount of liquid in the bottom stream increases thus increasing the bottom stream liquid volume fraction.

Further increase in the inlet flow rate results in a levelling off of the angular velocity as is predicted by the gompertz function used (see subsection 3.2.1). This function was tested against experimental data during the Specialization Project course in spring 2015 and shown to produce better model predictions. The levelling off has in this work been used to cater for mixing of already separated phases (re-entrainment) that would be expected at very high flow rates. The increase in inlet flow rate results in a decrease in droplet axial time and no further increase in droplet radial time because the angular velocity levels off. Therefore the liquid separation efficiency starts decreasing as is shown in sub-plot 2.

This decrease in separation efficiency translates to more liquid in the gas hence the gas volume fraction also decreases. In addition, the bottom stream liquid volume fraction also decreases because less liquid is separated from the gas.

For the same conditions and constant inlet flow rate, a decrease in split fraction from 0.85 to 0.7 does not affect both the angular velocity and liquid separation efficiency as is

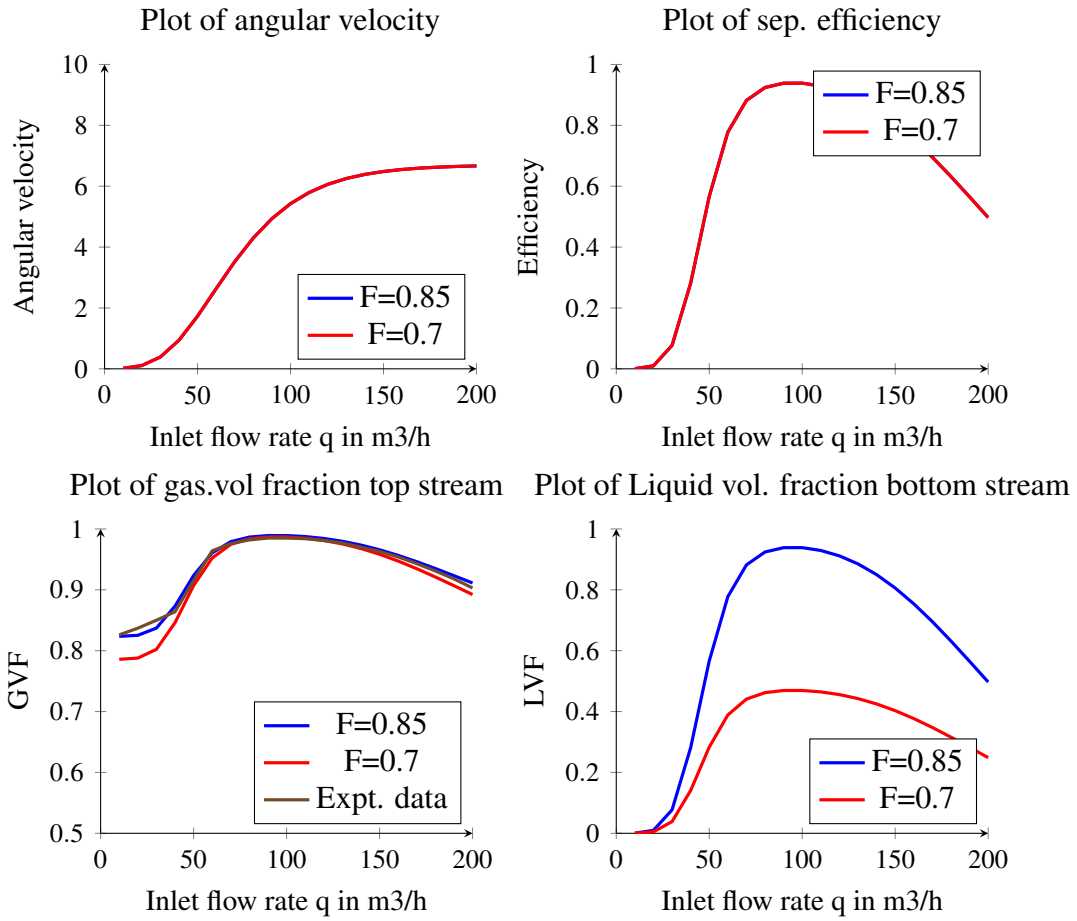

Figure 5.2: Deliquidizer performance-Inlet gas fraction f=0.85, Split fractions (top stream) F=0.85 & 0.7

The subplots 1,2,3,4 represent plots of angular velocity, liquid separation efficiency, top stream gas fraction and bottom stream liquid fraction respectively.

seen from sub-plots 1 and 2 in figure 5.2. However, the flow rate of the top outlet stream decreases without a change in separation efficiency and the amount of liquid separated. This implies a decrease in the amount of gas in the top stream since the amount of liquid remains unchanged thus the top stream gas volume fraction decreases hence the red curve being under the blue curve in sub-plot 3. In addition, the amount of gas to the bottom stream increases thus decreasing the liquid volume fraction. The magnitude of decrease is more pronounced in sub-plot 4 since the deliquidizer works on streams with high inlet gas and low liquid amounts.

5.1.3 Degasser

The Matlab code for this separator mod_degas.m is attached to Appendix A.1.4. The figure 5.3 below shows results for this separator. Low inlet flow rates generate low swirl intensities resulting in low angular velocities and ultimately low gas separation efficiencies since low centrifugal forces are generated.

Increasing the inlet flow rates results in increased angular velocities and hence better phase separation resulting in higher separation efficiencies. More gas is separated from liquid and hence the gas volume fraction of the top outlet stream increases as shown in sub-plot 3. In addition, the liquid volume fraction of the bottom outlet stream also increases because more gas is taken out of the liquid stream.

Further increase in the inlet flow rate results in a levelling off of the angular velocity as is predicted by the gompertz function. This results in a decrease in bubble axial time because the inlet flow rate increases and no further increase in bubble radial time. Therefore the separation efficiency decreases as is seen from sub-plot 2.

For a constant split fraction (F=0.2), because of the decrease in gas separation efficiency, the amount of liquid taken out at the top then increases therefore the gas volume fraction decreases. More gas remains in the liquid in the bottom stream thus the liquid volume fraction in this stream also decreases.

An increase in the split fraction from 0.2 to 0.4 for the same conditions and constant

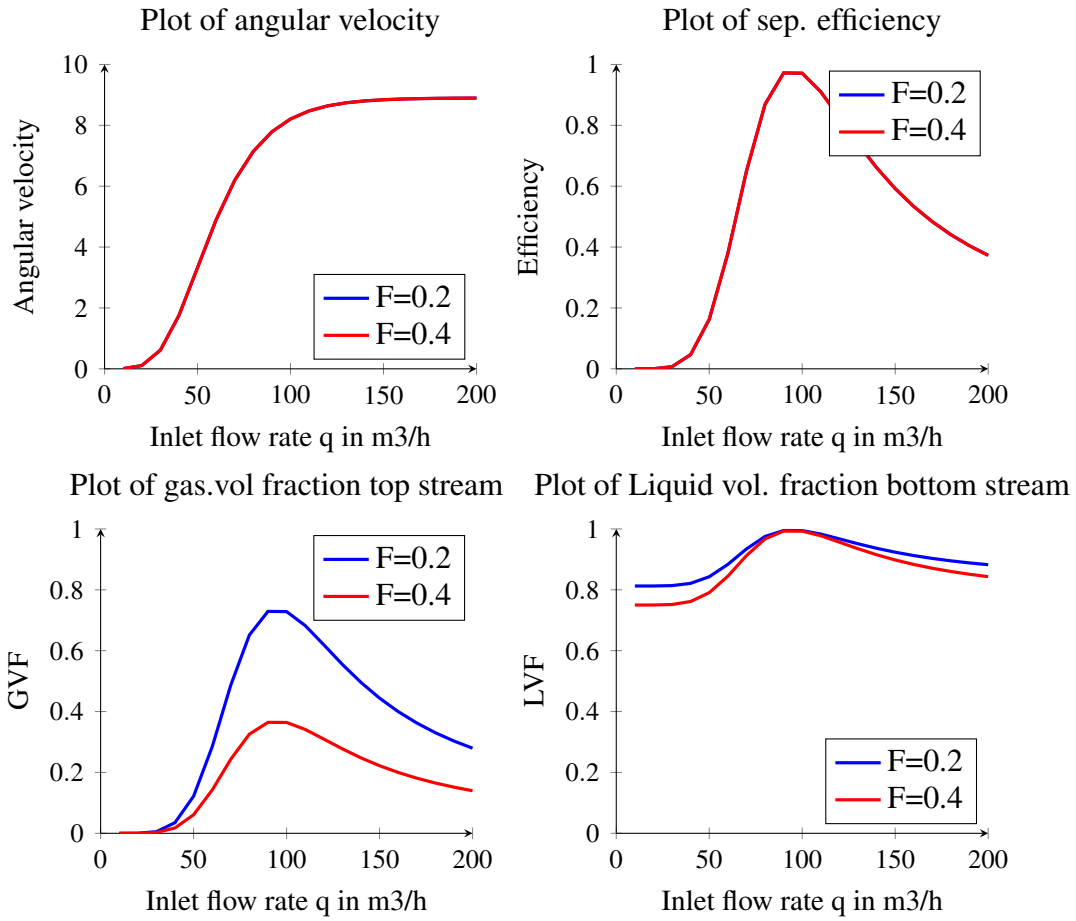

Figure 5.3: Degasser performance-Inlet gas fraction f=0.15, Split fractions (top stream) F=0.2 & 0.4

The subplots 1,2,3,4 represent plots of angular velocity, gas separation efficiency, top stream gas fraction and bottom stream liquid fraction respectively.

inlet flow rate does not affect both the angular velocity and gas separation efficiency as would be expected. Therefore, the top flow rate increases without an increase in the amount of gas separated. This means that more liquid is sucked into the top stream and therefore the gas volume fraction decreases as is seen from sub-plot 3 in figure 5.3. The liquid amount in the bottom stream decreases thus the liquid volume fraction also decreases.

5.1.4 Performance of the combined models

For clarity about the performance and effectiveness of the separation obtained by the models, the tables 5.2 to 5.4 below show the phase flow rates and balances around the separation units of the compact sub-sea separation system. A combined model for the separation system has been used with an inlet flow rate of 150 m^3/h, gas fraction 0.7 and top split fractions of 0.2 and 0.9 on the degasser and deliquidizer respectively. The combined model is attached to Appendix A.1 as mod_combined.m

Table 5.2: Performance of combined model-Gravity separator
Case ($q_1 = 150 m^3/h$, $f_1 = 0.7$, F1=0.2, F2=0.9)

Flow rate	Stream 1 (Inlet)	stream 2	stream 3	Balance(1-2-3)
Total	150	83.5	66.5	0
Gas	105	82.92	22.08	0
Liquid	45	0.58	44.42	0
Gas fraction	0.7	0.993	0.332	-

From table 5.2, we observe outlet streams with gas fractions of 0.993 for the top gas dominated stream and 0.332 for the bottom liquid dominated stream. This shows a reduction of liquid from a fraction of 0.3 in the inlet stream to 0.007 in the top outlet stream and a gas fraction reduction from 0.7 to 0.332 in the bottom outlet stream, hence separation. For comparison of the phase amounts than remain in outlet streams, more gas remains in the liquid stream as would be expected since the bubble rise velocities are smaller in magnitude due to a larger liquid viscosity in equation 3.25 than the liquid

terminal velocities given by equations 3.16 (smaller gas viscosity) and hence more gas is carried by the liquid.

Table 5.3: Performance of combined model-Degasser
Case ($q_1 = 150 m^3/h$, $f_1 = 0.7$, F1=0.2, F2=0.9)

Flow rate	Stream 3 (Inlet)	stream 4	stream 5	Balance(3-4-5)
Total	66.5	53.2	13.3	0
Gas	22.08	9.84	12.24	0
Liquid	44.42	43.36	1.06	0
Gas fraction	0.332	0.185	0.92	-

For the degasser, the liquid dominated stream enters with a gas fraction of 0.332 and exits with a fraction of 0.185. This represents a gas reduction of 55 % on the inlet amount and the top stream exits with a fraction of 0.92 with a low liquid amount. The gas separation efficiency is in close agreement to that from results presented in sub-plot 2 figure 5.3. However, better performance could be expected but is limited by the low inlet flow rate (66.5 m^3/h) translating into a low gas separation efficiency.

The inlet stream to the deliquidizer is a sum of streams 2 (from the gravity separator) and 5 (from the degasser). This is a gas dominated stream with a gas fraction of 0.983.

Table 5.4: Performance of combined model-Deliquidizer
Case ($q_1 = 150 m^3/h$, $f_1 = 0.7$, F1=0.2, F2=0.9)

Flow rate	Stream 6 (Inlet)	stream 7	stream 8	Balance(6-7-8)	stream 9
Total	96.8	87.1	9.7	0	62.9
Gas	95.16	87.0	8.16	0	18.0
Liquid	1.64	0.1	1.54	0	44.9
Gas fraction	0.983	0.999	0.84	-	0.286

Streams 7 and 9 are to compressor and pump respectively

The top stream exiting the deliquidizer has a gas fraction of 0.999 which represents a 94 % reduction on the incoming liquid amount. This liquid separation efficiency is in close agreement to the results as shown in sub-plot 2 figure 5.2 at an inlet flow rate of

96.8 m^3/h. This is also in agreement with Chin et al. (2003) who reports the inline deliquidizer to remove 90-95%+ of the upstream liquid. Stream 8 exits the boot section of the deliquidizer with a gas fraction of 0.84. This implies that the amount of gas to the pump becomes increased and hence a gas fraction of 0.286 in stream 9 to the pump. Note that stream 9 is combination of streams 4 and 8.

Overall, the gas stream 7 exits to the compressor with a liquid fraction of 0.001 and the liquid stream 9 to the pump, with a gas fraction of 0.286. Perhaps, a better performance is desired for this stream.

5.2 Optimization results

5.2.1 Results of optimization

There are 5 different optimization cases that were run in Matlab using the files optim.m, objfnc.m, confun.m attached in Appendix A.2 with fmincon as the solver and the solver settings are shown in table 5.5.

Table 5.5: Optimization settings for fmincon solver

Setting	Value
Algorithm	'sqp'
Max. function evaluations	200
Function tolerance	1e-6
Nonlinear constraint tolerance	1e-6

The Sequential quadratic programming ('sqp') algorithm was chosen after failure of the Interior Point algorithm. The Max. function evaluations are 100*numberOfVariables and the rest are default settings.

The optimization results are presented in table 5.6 below. Different initial guesses of the variables between 0 and 1 were tried and all found to result to the same optimal solution.

Table 5.6: Optimization results for the 5 different cases
Case2($+5\%\,q_1$), Case3($-5\%\,q_1$), Case4($+10\%\,f_1$) and Case5($-10\%\,f_1$)

Variables	Initial guess	Base-case	Case2	Case3	Case4	Case5
F1	0.2	0.3384	0.3898	0.2658	0.1327	0.3788
F2	0.6	0.9951	0.9939	0.9962	0.9937	0.9964
J	-	0.9748	0.9917	0.9483	0.8953	0.9877

5.2.2 Optimal performance

The optimal performance and effectiveness of the separation obtained for the base case is shown in tables 5.7 to 5.9 below with phase flow rates and balances around the separation units. The optimal case considered has an inlet flow rate of 150 m^3/h and gas fraction 0.65, and top split fractions of 0.3384 and 0.9951 on the degasser and deliquidizer respectively.

Table 5.7: Optimal performance-Gravity separator
Case ($q_1 = 150\,m^3/h$, $f_1 = 0.65$, F1=0.3384, F2=0.9951)

Flow rate	Stream 1 (Inlet)	stream 2	stream 3	Balance(1-2-3)
Total	150	67.2	82.8	0
Gas	97.5	66.73	30.77	0
Liquid	52.5	0.47	52.03	0
Gas fraction	0.65	0.993	0.372	-

From table 5.7, the outlet streams have gas fractions of 0.993 for the top gas dominated stream and 0.372 for the liquid dominated stream. This shows a reduction of liquid from a fraction of 0.35 in the inlet stream to 0.007 in the top outlet stream and a gas fraction reduction from 0.65 to 0.372 in the bottom outlet stream. This shows separation as would be expected but the amount of gas increases in the bottom stream. This is in agreement with the fact that a decrease in inlet gas fraction (from 0.7 for the combined model case to 0.65 for the optimal case) results in a decrease in gas separation efficiency as earlier discussed for the gravity separator results in figure 5.1.

Table 5.8: Optimal performance-Degasser

Case ($q_1 = 150 m^3/h$, $f_1 = 0.65$, F1=0.3384, F2=0.9951)

Flow rate	Stream 3 (Inlet)	stream 4	stream 5	Balance(3-4-5)
Total	82.8	54.78	28.02	0
Gas	30.77	2.76	28.01	0
Liquid	52.03	52.02	0.01	0
Gas fraction	0.372	0.05	1	-

For the degasser, the liquid dominated stream enters with a gas fraction of 0.372 and exits with a fraction of 0.05. This represents a gas reduction of 91 % on the inlet amount and the top stream exits with a gas fraction of 1 and ultimately a good separation performance.

Table 5.9: Optimal performance-Deliquidizer

Case ($q_1 = 150 m^3/h$, $f_1 = 0.65$, F1=0.3384, F2=0.9951)

Flow rate	Stream 6 (Inlet)	stream 7	stream 8	Balance(6-7-8)	stream 9
Total	95.22	94.75	0.47	0	55.25
Gas	94.74	94.74	0.0	0	2.76
Liquid	0.48	0.01	0.47	0	52.49
Gas fraction	0.995	0.999	0	-	0.05

Streams 7 and 9 are to compressor and pump respectively

The optimal performance of the deliquidizer shows a gas fraction of 0.999 for the top stream corresponding to a 98 % reduction on the incoming liquid amount and a bottom liquid stream exiting with no gas. In addition, stream 9 to the pump has a low gas content of 5%.

Overall, the gas stream 7 exits to the compressor with a liquid fraction of 0.001 and the liquid stream 9 to the pump, with a gas fraction of 0.05. Therefore, the separation performance of the optimal case is better than that of the non-optimal combined model case discussed in subsection 5.1.4.

5.2.3 Sensitivity analysis

The table 5.10 below shows the results for the sensitivity analysis on the optimum by parameters (inlet flow rate q_1 and inlet gas fraction f_1). Note that $S_P^C = \frac{\partial C^{opt}/C^{opt}}{\partial P/P}$.

Table 5.10: Sensitivity analysis

Cases	$S_{q_1}^J$	$S_{q_1}^{F1}$	$S_{q_1}^{F2}$	$S_{f_1}^J$	$S_{f_1}^{F1}$	$S_{f_1}^{F2}$
Case2	0.35	3.04	-0.02	-	-	-
Case3	0.54	4.29	-0.02	-	-	-
Case4	-	-	-	-0.82	-6.08	-0.01
Case5	-	-	-	-0.13	-1.19	-0.01

From table 5.10, we can conclude that changes in q_1 and f_1 have the largest relative influence on the optimum value of $F1$ with a small influence on the optimal objective function value J and a very low influence on $F2$. Therefore, precise values of q_1 and f_1 should be determined in order to find the true optimum.

6 Conclusion and Future work

6.1 Conclusion

The steady state models developed for the separation units of the compact sub-sea separation system have been shown to predict phase separation between gas and liquid phases and output stream flow rates and phase fractions. The trends of model results obtained are consistent with theoretical expectations.

Optimization on the system has been carried out and the results obtained have shown an average of not more than 5% of the dispersed phase in exit streams to the compressor and pump.

However, the lack of experimental data for the compact sub-sea separation system has been a major short coming in the validation of simulation results.

6.2 Future work

The models developed in this thesis do not account for the different flow regimes that are encountered for two-phase flow but assume a uniform regime of either annular or bubble flow. Therefore, the possibility of other regimes should later be considered.

We have assumed uniform droplet/ bubble size distributions for both the deliquidizer and degasser. However, the use of upper limit log normal distribution as used for the gravity separator may be considered in future work.

The gompertz function has been used in this report to represent angular velocity/ frequency in cyclonic separators. However, further studies about this representation should be considered.

We have assumed forced vortex flow in this thesis which is a good assumption only at the inlet but experimental studies have shown a combined vortex as the vortex associated

with cyclonic separation and should therefore be considered.

In addition, the strength of swirling flow decays along the cyclone length but this has not been considered in our model representations.

The validation of the model results presented in this thesis has been let down by the lack of experimental data. Thus, there is need to carry out experimental studies about the performance of these separation units.

Bibliography

Alary, V., Marchais, F., Palermo, T., et al., 2000. Subsea water separation and injection: A solution for hydrates. In: Offshore Technology Conference. Offshore Technology Conference.

Arpandi, I., Joshi, A., Shoham, O., Shirazi, S., Kouba, G., et al., 1996. Hydrodynamics of two-phase flow in gas-liquid cylindrical cyclone separators. SPE Journal 1 (04), 427–436.

Arpandi, I. A., 1995. A mechanistic model for two-phase flow in gas-liquid cylindrical cyclone separators. Ph.D. thesis, University of Tulsa.

Bothamley, M., et al., 2013a. Gas/liquid separators:quantifying separation performance-part 1. Oil and Gas Facilities 2 (04), 21–29.

Bothamley, M., et al., 2013b. Gas/liquid separators:quantifying separation performance-part 2. Oil and Gas Facilities 2 (05), 35–47.

Brenne, L., BjoÌÿrge, T., Bakken, L. E., Hundseid, O., 2008. Prospects for sub sea wet gas compression. In: ASME Turbo Expo 2008: Power for Land, Sea, and Air. American Society of Mechanical Engineers, pp. 671–677.

Chin, R., Stanbridg, D., Schook, R., et al., 2003. Development and installation of an inline deliquidiser. In: SPE Annual Technical Conference and Exhibition. Society of Petroleum Engineers.

Edgar, T. F., Himmelblau, D. M., Lasdon, L., 1989. Optimization of chemical processes. McGraw-Hill.

Ellingsen, C., 2007. Compact sub sea separation: Implementation and comparison of two different control structures. Master's thesis, Norwegian University of Science and Technology.

FMCtechnologies, February 2011. Compact total separation systems.
URL `www.fmctechnologies.com/separation`

Gomez, L., Mohan, R., Shoham, O., Kouba, G., et al., 2000. Enhanced mechanistic model and field-application design of gas/liquid cylindrical cyclone separators. Spe Journal 5 (02), 190–198.

Hamoud, A. A., Boudi, A. A., Al-Qahtani, S. D., 2009. New application of an inline separation technology in a real wet gas field. SAUDI ARAMCO JOURNAL OF TECHNOLOGY, 41.

Hinze, J., 1955. Fundamentals of the hydrodynamic mechanism of splitting in dispersion processes. AIChE Journal 1 (3), 289–295.

Hoffmann, A. C., Stein, L. E., 2002. Gas cyclones and swirl tubes. Springer-Verlag Berlin Heidelberg 2008.

Kataoka, I., Ishii, M., Mishima, K., 1983. Generation and size distribution of droplet in annular two-phase flow. Journal of Fluids Engineering 105 (2), 230–238.

Kouba, G., Shoham, O., 1996. A review of gas-liquid cylindrical cyclone (glcc) technology. In: Production Separation Systems International Conference, Aberdeen, England, April. pp. 23–24.

Kouba, G. E., Shoham, O., Shirazi, S., 1995. Design and performance of gas-liquid cylindrical cyclone separators. In: Proceedings of the BHR Group 7th International Meeting on Multiphase Flow, Cannes, France. pp. 307–327.

Marti, S., Erdal, F., Shoham, O., Shirazi, S., Kouba, G., 1996. Analysis of gas carry-under in gas-liquid cylindrical cyclones. In: Hydrocyclones 1996 International Meeting, St. John College, Cambridge, England, April. pp. 2–4.

Mokhatab, S., Poe, W. A., 2012. Handbook of natural gas transmission and processing. Gulf Professional Publishing.

Monsen, G. O. T., 2012. Modeling of a centrifugal separator for dispersed gas-liquid flows.

Movafaghian, S., Jaua-Marturet, J., Mohan, R. S., Shoham, O., Kouba, G., 2000. The effects of geometry, fluid properties and pressure on the hydrodynamics of gas–liquid cylindrical cyclone separators. International Journal of Multiphase Flow 26 (6), 999–1018.

Pan, L., Hanratty, T. J., 2002. Correlation of entrainment for annular flow in horizontal pipes. International journal of multiphase flow 28 (3), 385–408.

Pereyra, E., Gomez, L., Mohan, R., Shoham, O., Kouba, G., 2009. Transient mechanistic model for slug damper/gas-liquid cylindrical cyclone (glcc©) compact separator system. In: ASME 2009 28th International Conference on Ocean, Offshore and Arctic Engineering. American Society of Mechanical Engineers, pp. 661–672.

Rangaiah, G. P., Kariwala, V., 2012. Plantwide control: Recent developments and applications. John Wiley & Sons.

Sayda, A. F., Taylor, J. H., 2007. Modeling and control of three-phase gravilty separators in oil production facilities. In: American Control Conference, 2007. ACC'07. IEEE, pp. 4847–4853.

Schook, R., van Vorselen, M., et al., 2005. Compact separation by means of inline technology. In: Offshore Mediterranean Conference and Exhibition. Offshore Mediterranean Conference.

Simmons, M. J., Hanratty, T. J., 2001. Droplet size measurements in horizontal annular gas–liquid flow. International journal of multiphase flow 27 (5), 861–883.

Skogestad, S., 2004. Near-optimal operation by self-optimizing control: From process control to marathon running and business systems. Computers & chemical engineering 29 (1), 127–137.

Stene, M., 2013. Cfd study of a rotating gas-liquid separator: Design og bygging av flere mikro-dråpe generatorer.

Swanborn, R. A., 1988. A new approach to the design of gas-liquid separators for the oil industry. Univerity of Delft.

Van Campen, L., 2014. Bulk dynamics of droplets in liquid-liquid axial cyclones. Ph.D. thesis, TU Delft, Delft University of Technology.

van Wissen, R., Brouwers, J., Golombok, M., 2007. In-line centrifugal separation of dispersed phases. AIChE journal 53 (2), 374–380.

A Appendix

A.1 Matlab model codes

A.1.1 par_css.m

```
function p = par_css()
% Parameters for compact separation system
%
p.rho_g=15.7; % density of gas corrected to 25 bar.
p.rho_l=850; % 35 API gravity crude oil- dens_liq kg/m3
p.mu_g=1.83e-05; % visco_gas kg/m/s
p.mu_l=16.7e-03; % visco_liq kg/m/s
p.D=0.1; % Diameter inlet pipe in m
p.Dg=1; % Diameter of gravity sep
p.g=9.81;
p.surf_t=0.032; % Liq surf tension in N/m
p.Em=0.99; % maximum entrainment fraction
p.m=1; % settling law exponent
p.delta=0.72;

p.R=9e-02; % radius of degasser
p.r_g=sqrt(0.18)*p.R; % radius of gas extr. pipe
p.L_2=2;% length of degasser
p.dp=250*1e-06; % droplet size

p.R_3=7.5e-02; % radius of deliquidizer
p.L_3=1.5;% length of deliquidizer

end
```

A.1.2 mod_grav.m

```
function [q_2,f2,q_3,beta_3]=mod_grav(q_1,f1)
%% Gravity separator model predicting
% outlet flow rates and phase fractions

% Parameters
p = par_css(); % parameter function

% Input
% q_1 is inlet flow rate
% f1 is inlet gas fraction

v_dot=q_1./3600;
q_g1=f1*v_dot;
q_l1=(1-f1)*v_dot;
ug=(4*q_g1)./(pi*p.D^2); % gas velocity
ul=(4*q_l1)./(pi*p.D^2); % liq velocity

% Inlet liquid entrainment E
% Calculate d32

d32=((0.0091*p.surf_t.*p.D)./(p.rho_g*ug.^2)).^0.5; % in m

% Calculate E
B=9*(p.D*ug.^3*sqrt(p.rho_l*p.rho_g)/p.surf_t).*((p.rho_g^(1-p.m)*...
p.mu_g^p.m)./(d32.^(1+p.m)*p.g*p.rho_l)).^(1/(2-p.m));
E=(B./(1+B))*p.Em;

% Normalized and cumulative vol. distribution of entrained liquid.
% Calculate dv50 in microns;
Re=p.D.*ug*p.rho_g/p.mu_g;
dv50=0.01*(p.surf_t./(p.rho_g*ug.^2)).*(Re).^(2/3)*...
(p.rho_g/p.rho_l)^(-1/3)*(p.mu_g/p.mu_l)^(2/3);
dv50=dv50*10^6;
dmax=5*dv50;
a=(dmax-dv50)/dv50;

% Separation
% Calculate dp_cut (sizes > dp_cut are separated)
```

```
% Equating the terminal droplet and gas velocities
dp_cut=((4*18*p.mu_g*q_g1)./(pi*p.Dg^2*p.g*(p.rho_l-p.rho_g)))...
.^0.5*10^6;
z_cut=log(a.*dp_cut./(dmax-dp_cut));

Beta=1-0.5*(1-erf(p.delta*z_cut)); % Fract.entrained liq in exit gas
% Sep. efficiency liq
sep_eff=(1-Beta)*100;

%% Gas entrainment
% Calculate d32g
d32g=((0.0091*p.surf_t.*p.D)./(p.rho_l*ul.^2)).^0.5; % in m

% Calculate Eg
Bg=9*(p.D*ul.^3*sqrt(p.rho_l*p.rho_g)/p.surf_t).*((p.rho_l^...
(1-p.m)*p.mu_l^p.m)./(d32g.^(1+p.m)*p.g*p.rho_l)).^(1/(2-p.m));
Eg=(Bg./(1+Bg))*p.Em;

% Normalized and cumulative vol. distribution of entrained gas.
Reg=p.D.*ul*p.rho_l/p.mu_l;
dv50g=0.01*(p.surf_t./(p.rho_l*ul.^2)).*(Reg).^(2/3)*...
(p.rho_l/p.rho_g)^(-1/3)*(p.mu_l/p.mu_g)^(2/3);
dv50g=dv50g*10^6;
dmaxg=5*dv50g;
ag=(dmaxg-dv50g)/dv50g;

% Separation
dp_cutg=((4*18*p.mu_l*q_l1)./(pi*p.Dg^2*p.g*(p.rho_l-p.rho_g)))...
.^0.5*10^6;
z_cutg=log(ag.*dp_cutg./(dmaxg-dp_cutg));
Betag=1-0.5*(1-erf(p.delta*z_cutg));

% Sep. efficiency gas
sep_effg=(1-Betag)*100;

% Exiting stream flow rates and fractions
q_l2=Beta.*E.*(1-f1).*q_1; % liq out top
q_l3=(1-f1).*q_1-q_l2; % liq out bottom
```

```
q_g3=Betag.*Eg.*f1.*q_1; % gas out bottom
q_g2=f1.*q_1-q_g3; % gas out top

q_3=q_g3+q_l3; % Bottom flow rate
q_2=q_g2+q_l2; % Top flow rate

f2=q_g2./q_2; % top gas fraction
beta_3=q_l3./(q_g3+q_l3); % Bottom liq fraction

% data_grav=[q_1' E' Eg' sep_eff' sep_effg' f2' beta_3'];
% save grav.dat data_grav -ASCII

% Plotting
figure(1)
subplot(3,2,1)
plot(q_1,E)
title('Plot of liquid entrainment fraction')
xlabel('Inlet flow rate m3/h')
ylabel('Entrainment fraction E')
grid on

subplot(3,2,2)
plot(q_1,Eg)
title('Plot of gas entrainment fraction')
xlabel('Inlet flow rate m3/h')
ylabel('Entrainment fraction Eg')
grid on

subplot(3,2,3)
plot(q_1,sep_eff)
title('Plot of Liquid separation efficiency')
xlabel('Inlet flow rate m3/h')
ylabel('Sep. eff.-liquid')
grid on

subplot(3,2,4)
plot(q_1,sep_effg)
title('Plot of gas separation efficiency')
```

```
xlabel('Inlet flow rate m3/hr')
ylabel('Sep. eff.-gas')
grid on

subplot(3,2,5)
plot(q_1,f2)
title('Plot of gas vol fraction top exiting stream')
xlabel('Inlet flow rate m3/h')
ylabel('Gas vol. fraction')
grid on

subplot(3,2,6)
plot(q_1,beta_3)
title('Plot of Liquid vol fraction bottom exiting stream')
xlabel('Inlet flow rate m3/h')
ylabel('Liq.vol. fraction ')
grid on

% balances
bal_g=f1*q_1-q_g2-q_g3
bal_l=(1-f1)*q_1-q_l2-q_l3

end
```

A.1.3 mod_deliq.m

```
function [q_top,alpha,q_bottom,beta]=mod_deliq(Qi,f,F3)

%%  Final deliquidizer model

% Parameters
p = par_css(); % parameter function

% Input
% f is fraction of gas
% F3 split fraction top
```

```
% Qi Inlet vol. flowrate in m3/h

dp_d=-0.6*(Qi)*1e-06 + 0.0002; % Droplet size
vdot=(Qi)/3600;% in m3/s
w=6.7*exp(-8.7*exp(-0.0372*Qi));
t_axial= (pi*p.R_3^2*p.L_3)./vdot;

y=(log(p.R_3)-(t_axial.*(dp_d.^2)*(p.rho_l-p.rho_g).*...
(w.^2))/(18*(p.mu_g)));
r_l=exp(y);
sep_eff=(1-(r_l/p.R_3).^2);
q_lsep=(1-f)*Qi.*(1-(r_l/p.R_3).^2); % liq sep

% Specify top flow rate deliquidizer

q_top=F3.*Qi;
q_lot=(1-f)*Qi-q_lsep;
q_got=q_top-q_lot;

alpha=q_got./q_top;

% Out of boot

q_bottom=Qi-q_top;
q_lob=(1-f)*Qi-q_lot;
q_gob=q_bottom-q_lob;

beta=q_lob./q_bottom;

% Experimental data for comparison
alpha_g=[0.826 0.837 0.850 0.864 0.915 0.964 0.976 0.982 0.985...
0.985 0.984 0.981 0.977 0.970 0.963 0.954 0.943 0.931 0.918 0.903 ];

% Save data for plotting
% data_deliq=[Qi' w' sep_eff' alpha' alpha_g' beta']
% save deliq.dat data_deliq -ASCII

% Plotting
```

```
figure(1)
subplot(2,2,1)
plot(Qi,w)
title('Plot of angular velocity')
xlabel('total volumetric flowrate Qi in m3/h')
ylabel('angular velocity, w')
grid on

subplot(2,2,2)
plot(Qi,sep_eff)
title('Plot of sep. eff liq')
xlabel('total volumetric flowrate Qi in m3/h')
ylabel(' Liq sep.eff')
grid on

subplot(2,2,3)
plot(Qi,alpha)
title('Plot of quality of gas')
xlabel('total volumetric flowrate Qi in m3/h')
ylabel('quality of gas, alpha')
grid on

% hold on
% scatter(Qi,alpha_g,'.') % data points for comparison
% legend('GVF','data','Location','SouthEast')

subplot(2,2,4)
plot(Qi,beta)
title('Plot of quality of liquid')
xlabel('total volumetric flowrate Qi in m3/h')
ylabel('quality of liquid, beta')
grid on

% check balances
bal_g=f*Qi-q_got-q_gob
bal_l=(1-f)*Qi-q_lot-q_lob
```

```
end
```

A.1.4 mod_degas.m

```
function [q_5,f5,q_4,beta_4]=mod_degas(q_3,beta_3,F2)

%% Final model degasser

% Parameters
p = par_css(); % parameter function

% Input
% q_3 Inlet flow rate
% beta_3 Input liq. vol. fraction
% F2 Split fraction top stream

vdot2=q_3./3600;% in m3/s
w=8.9*exp(-12*exp(-0.05.*q_3));
t_axial= (pi*p.R^2*p.L_2)./vdot2;

% Forced vortex(Solid body)
y=(log(p.r_g) - 4*(pi)^2*(t_axial.*(p.dp.^2)*...
(p.rho_g-p.rho_l).*(w.^2))/(18*p.mu_l));
r_l=exp(y);

eff=((r_l.^2-p.r_g^2)./(p.R^2-p.r_g^2));
q_gsep=(1-beta_3)*q_3.*((r_l.^2-p.r_g^2)./(p.R^2-p.r_g^2));% gas sep.

% Exiting streams
q_5=F2.*q_3; % top flow rate
q_l5=q_5-q_gsep; % liq out top
q_g5=q_5-q_l5; % gas out top

q_4=(1-F2).*q_3; % bottom flow rate

q_l4=beta_3*q_3-q_l5; % liq out bottom
```

```
q_g4=(1-beta_3).*q_3-q_gsep; % gas out bottom

f5=q_g5./q_5; % gas fraction top
beta_4=q_l4./(q_4); % liq fraction bottom

% data_deg=[q_3' w' eff'  f5' beta_4'];
% save deg.dat data_deg -ASCII

% Plotting

figure(1)
subplot(2,2,1)
plot(q_3,w)
title('Plot of angular velocity')
xlabel('Inlet flowrate Qi in m3/h')
ylabel('angular velocity, w')
grid on

subplot(2,2,2)
plot(q_3,eff)
title('Plot of gas sep efficiency')
xlabel('Inlet flowrate Qi in m3/h')
ylabel('sep.eff')
grid on

subplot(2,2,3)
plot(q_3,f5)
title('Plot of gas quality top stream')
xlabel('Inlet flowrate Qi in m3/h')
ylabel('quality of gas, alpha')
grid on

subplot(2,2,4)
plot(q_3,beta_4)
title('Plot of liquid quality bottom stream')
xlabel('Inlet flowrate Qi in m3/h')
ylabel('quality of liquid, Beta_l')
grid on
```

```
% balances
bal_g=(1-beta_3)*q_3-q_g5-q_g4
bal_l=beta_3*q_3-q_l5-q_l4

end
```

A.1.5 mod_combined.m

```
function [q_7,f7,q_9,beta_9]=mod_comp(q_1,f1,F2,F3)
%% Combined model
% q_1 inlet flow rate
% f1 inlet gas fraction
% F2, F3 top split fractions
% on degasser and deliquidizer

% Parameters
p = par_css(); % parameter function

% Grav sep
[q_2,f2,q_3,beta_3]=mod_grav(q_1,f1)

% Degas
[q_5,f5,q_4,beta_4]=mod_degas(q_3,beta_3,F2)

q_6=q_2 +q_5
q_g6=f2.*q_2 + f5.*q_5;
q_l6=(1-f2).*q_2 +(1-f5).*q_5;

f6=q_g6./q_6

% Deliq
[q_7,f7,q_8,beta_8]=mod_deliq(q_6,f6,F3)

% To pump
q_g9=(1-beta_4).*q_4 + (1-beta_8).*q_8;
```

```
q_l9=beta_4.*q_4 + beta_8.*q_8;
q_9=q_g9 + q_l9;
beta_9=q_l9./q_9;

end
```

A.2 Matlab optimization codes

A.2.1 optim.m

```
%% Optimization script
clear
clc
l=0.1:0.1:0.9; % All guesses
optimal_soln=zeros(length(l),3);

for i=1:length(l)
x0=[l(i),l(i)];% x0

% Inequality linear constraints form A.x<=b
b=[1;-0;1;-0];
A=[1 0 ;-1 0 ;0 1 ;0 -1];

options = optimset('TolFun',1e-6,'TolCon',1e-6,'MaxFunEvals'...
,200,'Display','iter','Algorithm','sqp','Diagnostics','on');

[x,fval,exitflag,output,lambda,grad,hessian]=...
fmincon(@objfnc,x0,A,b,[],[],[],[],@confun,options);

optimal_soln(i,:)=[x -fval];
end

optimal_soln
```

A.2.2 objfnc.m

```
function [beta_alpha]=objfnc(x)
%% Objective fnc
% q_1 inlet flow rate
% f1 inlet gas fraction
% F2, F3 top split fractions
% on degasser and deliquidizer

% Parameters
p = par_css(); % parameter function

F2=x(1);
F3=x(2);

q_1=100; %inlet flow rate in m3/h
f1=0.7; % inlet gas fraction

% Grav sep
[q_2,f2,q_3,beta_3]=mod_grav(q_1,f1);

% Degas
[q_5,f5,q_4,beta_4]=mod_degas(q_3,beta_3,F2);

q_6=q_2 +q_5;
q_g6=f2.*q_2 + f5.*q_5;
q_l6=(1-f2).*q_2 +(1-f5).*q_5;
f6=q_g6./q_6;

% Deliq
[q_7,f7,q_8,beta_8]=mod_deliq(q_6,f6,F3);

% To pump
q_g9=(1-beta_4).*q_4 + (1-beta_8).*q_8;
q_l9=beta_4.*q_4 + beta_8.*q_8;
q_9=q_g9 + q_l9;
```

```
beta_9=q_l9./q_9;
beta_alpha=-(beta_9 + f7)./2;

end
```

A.2.3 confun.m

```
function [c,ceq]=confun(x)
%% nonlinear constraints
% Parameters
p = par_css(); % parameter function

F2=x(1);
F3=x(2);

q_1=100; % inlet flow rate m3/h
f1=0.7; % inlet gas fraction

% Grav sep
[q_2,f2,q_3,beta_3]=mod_grav(q_1,f1);

c(1)=[f2-1];
c(2)=[beta_3-1];
c(3)=[-(1-beta_3).*q_3]; % q_g3

% Degas
[q_5,f5,q_4,beta_4]=mod_degas(q_3,beta_3,F2);

c(4)=[-(1-f5).*q_5]; % q_l5
c(5)=[f5-1];
c(6)=[beta_4-1];

q_6=q_2 +q_5;
q_g6=f2.*q_2 + f5.*q_5;
q_l6=(1-f2).*q_2 +(1-f5).*q_5;
```

```
f6=q_g6./q_6;
c(7)=[f6-1];

% Deliq
[q_7,f7,q_8,beta_8]=mod_deliq(q_6,f6,F3);

c(8)=[f7-1];
c(9)=[-(1-beta_8).*q_8]; % q_g8

% To pump
q_g9=(1-beta_4).*q_4 + (1-beta_8).*q_8;
q_l9=beta_4.*q_4 + beta_8.*q_8;
q_9=q_g9 + q_l9;
beta_9=q_l9./q_9;
beta_alpha=-(beta_9 + f7)./2;

ceq = []; % non-linear equality constraints

end
```